LEVEL II

AFWAL-TR-80-3090

AD A101494

FINITE SPAN EFFECTS ON FLAP HEATING AND
EFFECTIVENESS IN A TURBULENT BOUNDARY LAYER

L. A. CASSEL
L. D. MC MILLEN
S. TAYLOR

JUL 17 1981

E

SCIENCE APPLICATIONS, INC.- AERONAUTICAL SYSTEMS TECHNOLOGY DIVISION

17900 Skypark Circle, Irvine, California 92714 (714) 641-1591

AUGUST 1980

TECHNICAL REPORT AFWAL-TR-80-3090

Final Report for May 1978 - December 1980

Approved for public release; distribution unlimited.

FLIGHT DYNAMICS LABORATORY
AIR FORCE WRIGHT AERONAUTICAL LABORATORIES
AIR FORCE SYSTEMS COMMAND
WRIGHT-PATTERSON AIR FORCE BASE, OHIO 45433

81 7 13 045

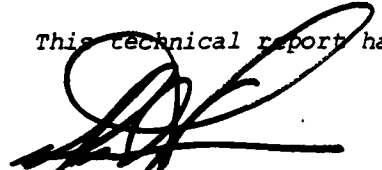DTIC FILE COPY

RICHARD D. NEUMANN
Project Engineer
Aerodynamic Heating Group

MELVIN L. BUCK
Chief, High Speed Aero Perf. Branch
Aeromechanics Division

FOR THE COMMANDER

PETER J. BUTKEWICZ, COL, USAF
Chief, Aeromechanics Division
AF Wright Aeronautical Laboratories (AFSC)

REPORT DOCUMENTATION PAGE		READ INSTRUCTIONS BEFORE COMPLETING FORM
1. REPORT NUMBER AFWAL-TR-80-3090	2. GOVT ACCESSION NO. AD-A1C1 494	3. RECIPIENT'S CATALOG NUMBER
4. TITLE (and Subtitle) FINITE SPAN EFFECTS ON FLAP HEATING AND EFFECTIVENESS IN A TURBULENT BOUNDARY LAYER		5. TYPE OF REPORT & PERIOD COVERED FINAL TECHNICAL MAY 1978 TO DECEMBER 1980
		6. PERFORMING ORG. REPORT NUMBER
7. AUTHOR(s) L. A. CASSEL L. D. MC MILLEN S. TAYLOR		8. CONTRACT OR GRANT NUMBER(s) F33615-78-C-3001
9. PERFORMING ORGANIZATION NAME AND ADDRESS SCIENCE APPLICATIONS, INC. AERONAUTICAL SYSTEMS TECHNOLOGY DIVISION 17900 SKYPARK CIRCLE, IRVINE, CA 92714		10. PROGRAM ELEMENT, PROJECT, TASK AREA & WORK UNIT NUMBERS PROJECT 2404 TASK NO. 24040 WORK UNIT NO. 24040718
11. CONTROLLING OFFICE NAME AND ADDRESS FLIGHT DYNAMICS LABORATORY AIR FORCE WRIGHT AERONAUTICAL LABORATORIES AIR FORCE SYSTEMS COMMAND WRIGHT-PATTERSON AIR FORCE BASE, OH 45433		12. REPORT DATE AUGUST 1980
		13. NUMBER OF PAGES 63
14. MONITORING AGENCY NAME & ADDRESS(if different from Controlling Office)		15. SECURITY CLASS. (of this report) UNCLASSIFIED
		15a. DECLASSIFICATION DOWNGRADING SCHEDULE

16. DISTRIBUTION STATEMENT (of this Report)

APPROVED FOR PUBLIC RELEASE: DISTRIBUTION UNLIMITED

17. DISTRIBUTION STATEMENT (of the abstract entered in Block 20, if different from Report)

18. SUPPLEMENTARY NOTES

19. KEY WORDS (Continue on reverse side if necessary and identify by block number)

EXPERIMENT
FINITE SPAN FLAP
SUPERSONIC/HYPERSONIC
2-D BODY

TURBULENT BOUNDARY LAYER
ATTACHED COMPRESSION
FLAP HEATING
FLAP PRESSURES

20. ABSTRACT (Continue on reverse side if necessary and identify by block number)

An experiment was conducted in the NASA Langley Continuous Flow Hypersonic Tunnel to measure the heat transfer and pressure distributions on finite span flaps subjected to turbulent boundary layer conditions. Data were obtained for three span widths at deflection angles below that required to induce separation at the compression corner. The results are compared with other experimental data and theoretical predictions.

DD FORM 1473 1 JAN 73   EDITION OF 1 NOV 65 IS OBSOLETE

412433

PREFACE

This report was prepared for the Air Force Wright Aeronautical Laboratories, Wright-Patterson Air Force Base, Ohio, under contract number F33615-78-C-3001. The contract was initiated under project number 2404, task number 240407 and work unit number 24040718. The work was performed by the Aeronautical Systems Technology Division, Science Applications, Inc. (SAI) in Irvine, California as part of the Hypersonic Aeromechanics Technology (HAT) program. The HAT program was initiated in May 1978 and completed in December 1980. Mr. R. D. Neumann was the Air Force Project Engineer. Mr. L. A. Cassel was the SAI Program Manager for the period May 1978 to December 1979 and Mr. S. Taylor assumed the responsibilities from January 1980. The principal investigators were Mr. L. A. Cassel and Dr. L. D. McMillen.

The authors gratefully acknowledge the contributions of Mr. R. D. Neumann whose discussion and guidance throughout the conduct of this study were helpful in the successful completion of the task and report. The authors wish to also thank Mr. Tom Jarrett, the SAI test monitor, and Mr. Tom Blackstock, the NASA Langley Research Center test engineer at the Continuous Flow Hypersonic Tunnel, for their contributions to the successful conduction of the test program. Finally, we also thank Mr. J. C. Courtney, SAI, and Mrs. K. A. Mamelli, SAI, for their contributions in the preparation of this report.

A test data report, AFWAL-TM-80-62-FIMG, "Finite Span Effects on Flap Heating and Effectiveness in a Turbulent Boundary Layer - Test Data Report", was also prepared under the subject contract, by T. W. Jarrett, L. A. Cassel, and L. D. McMillen, April 1980.

Accession For	
NTIS GRA&I	X
DTIC TAB	[ ]
Unannounced	[ ]
Justification	
By	
Distribution /	
Availability Codes	
Dist	Avail and/or Special
A	

iii

TABLE OF CONTENTS

LIST OF ILLUSTRATIONS

LIST OF SYMBOLS

b_f	flap span, in.
c_p	specific heat, BTU/lbm°R
C_p	pressure coefficient
D_N	leading edge diameter, in.
g	gravitational acceleration, ft/sec^2
h	heat transfer coefficient, BTU/ft^{2}sec°R
M	Mach number
N	Normal force on flap surface, lb.
p	pressure, psia or atm.
p_t	total pressure, psia or atm.
$\dot{q}$	heat transfer rate, BTU/ft^{2}sec
Re	Reynolds number per foot, ft^{-1}
Re_x	running length Reynolds number
R_N	leading edge cylindrical radius, in.
S_t	Stanton number
t	time, sec.
T	temperature, °R
u	velocity, ft/sec
u_τ	shear velocity, ft/sec
X	distance from leading edge of plate, in.
X_t	transition running length, in.
Y	normal coordinate in boundary layer, in.
Z	distance from flap edge, in.
α	plate angle of attack, deg.
β	shock angle, deg.

LIST OF SYMBOLS (Continued)

δ	boundary layer thickness, in.
ΔX	distance from compression corner, in.
λ	flap deflection angle, deg.
μ	viscosity, lb-sec/ft^2 or Mach angle, $\sin^{-1}\left(\frac{1}{M}\right)$
ρ	density, lbm/ft^3
τ	shear force, lb/ft^2

Subscripts

1	condition upstream of flap shock
2	downstream of flap shock
c	compression corner
e	boundary layer edge quantity
i	inviscid condition
m	measured value
mm	model material
r	recovery condition
t	total condition
w	value at the wall
∞	freestream value
o	total condition

Superscripts

*	reference enthalpy condition
-	equivalent incompressible value

SECTION I

INTRODUCTION

Trailing edge flaps are favored control concepts for a wide range of advanced hypersonic missiles, aircraft and reentry vehicles. The design of these controls and evaluation of their effectiveness is a continuing contemporary problem in hypersonic flight vehicle development. Fundamental to the design process is the prediction of heat transfer and pressure distributions over the flap surface. Three design parameters are of interest. The integral of the pressure distribution provides the control forces. The moment of that integral, termed the hinge moment, is required to design actuator systems and predict dynamics. Finally, the magnitude and variation in heat transfer are required to design thermal protection systems.

Critical flap design environments generally occur at high dynamic pressure conditions, such that the boundary layer approaching the flap is turbulent. Since the performance of the flap is highly sensitive to the nature of the upstream boundary layer, it is essential that analytic and experimental investigations of flap performance properly characterize the in-flight boundary layer state. Unfortunately, Reynolds number limitations in existing ground test facilities often preclude successful attainment of "naturally" turbulent boundary layers upstream of controls on scaled models of flight vehicles. This is particularly true when the flap chord dimension is the same order of magnitude as the approaching boundary layer thickness, which is a common design condition. As a result, boundary layer transition in ground test facilities is most often accomplished through the employment of boundary layer trips. This procedure alters the natural growth of the turbulent boundary layer and may introduce significant error into the simulation of flow over the flap. Consequently, a source of data defining the behavior of pressure and heat transfer distributions on control surfaces for naturally turbulent upstream flow conditions is a valuable aid to the design aerodynamicist.

1

The great majority of prior experimental (and analytic) efforts applicable to flap design and performance have focused primarily on the separated flow problem, with emphasis on the characterization of incipient separation conditions. Those efforts which have dealt with turbulent boundary layers have, for the most part, been constrained to the two dimensional problem, i.e., they have modeled the effectively infinite span flap, and have produced results characterizing performance at relatively high deflection angles. The effort reported here was directed toward an evaluation of compression flap performance at deflection angles below those required to induce turbulent boundary layer separation. An experiment was conducted to measure surface pressure and heat transfer distributions on finite span flaps in approaching two-dimensional, naturally turbulent, attached flow conditions. Chordwise and spanwise variations in pressures and heat transfer rates were measured as functions of flap deflection angle. The experiment was conducted in the Continuous Flow Hypersonic Tunnel (CFHT) at the National Aeronautics and Space Agency (NASA) Langley Research Center (LaRC).

SECTION II

EXPERIMENTAL DESCRIPTION

2.1 Test Facility Description

The Langley Research Center Continuous Flow Hypersonic Tunnel (LaRC CFHT) was used to conduct this experiment in an intermittent or blowdown mode. A photograph of the test facility is presented in Figure 1. The fixed nozzle transitions from a circular throat to a 31.0 in. square test section which was operated at a nominal freestream Mach number of M_∞ = 10. The working fluid was air which was heated, after compression, by electrical resistance tube bundles to avoid liquification. The nominal reservoir conditions were $(P_0)_\infty$ = 1650 psia (112.3 atm) stagnation pressure and $(T_0)_\infty$ = 1760°R stagnation temperature, providing a freestream Reynolds number of 2.19 x 10^6 per foot and M_∞ = 10.19. A more complete description of the facility is available in Reference 1.

2.2 Models

The basic flat plate model with interchangeable flaps and leading edge components is shown in Figure 2. The aftmost section of the plate sloped downward from the primary surface, across its span, at a 15 degree angle starting at the flap leading edge. The streamwise centerline of each of the three flaps tested -- 5.0, 4.0, and 2.0 in. in width, and all with 4.0 in. chord lengths, coincided with the centerline of the primary surface. Appropriate plates were employed to position the flaps at incidence angles of 0, 5, 10 or 15 degrees. Also shown in Figure 2 are the three leading edges used in the test, representing sharp and cylindrically blunted wedges. Post test measurement of the sharp leading edge indicated that the diameter was .037 ± .003 in. The radii of the other leading edges were 0.5 and 1.0 in.

The required overall model length (36 in.) was approximately 6 in. longer than the length of a plate which could be physically injected into the tunnel. To overcome this constraint, the model was designed with
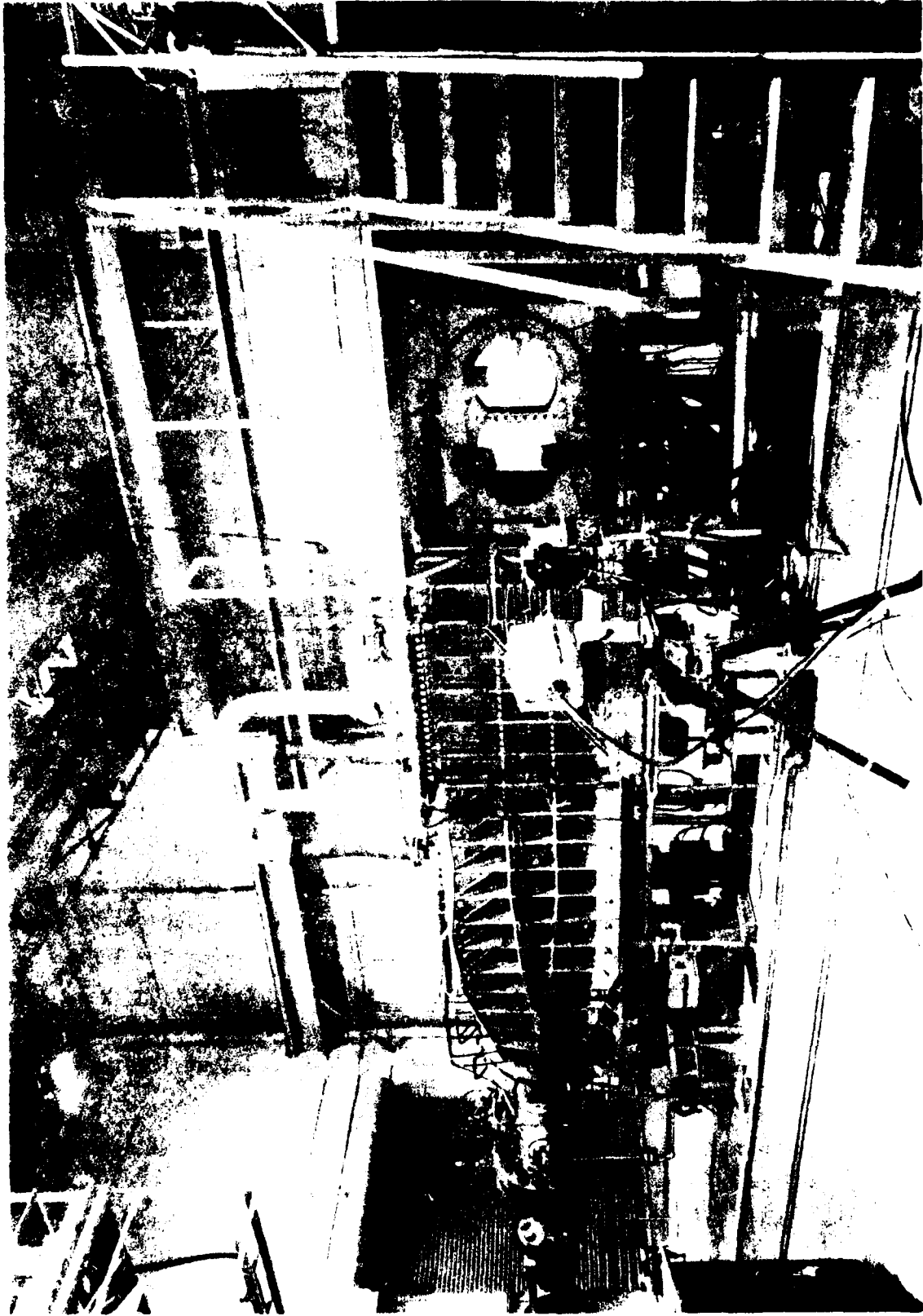
FIGURE 1. THE LaRC CONTINUOUS FLOW HYPERSONIC TUNNEL

4
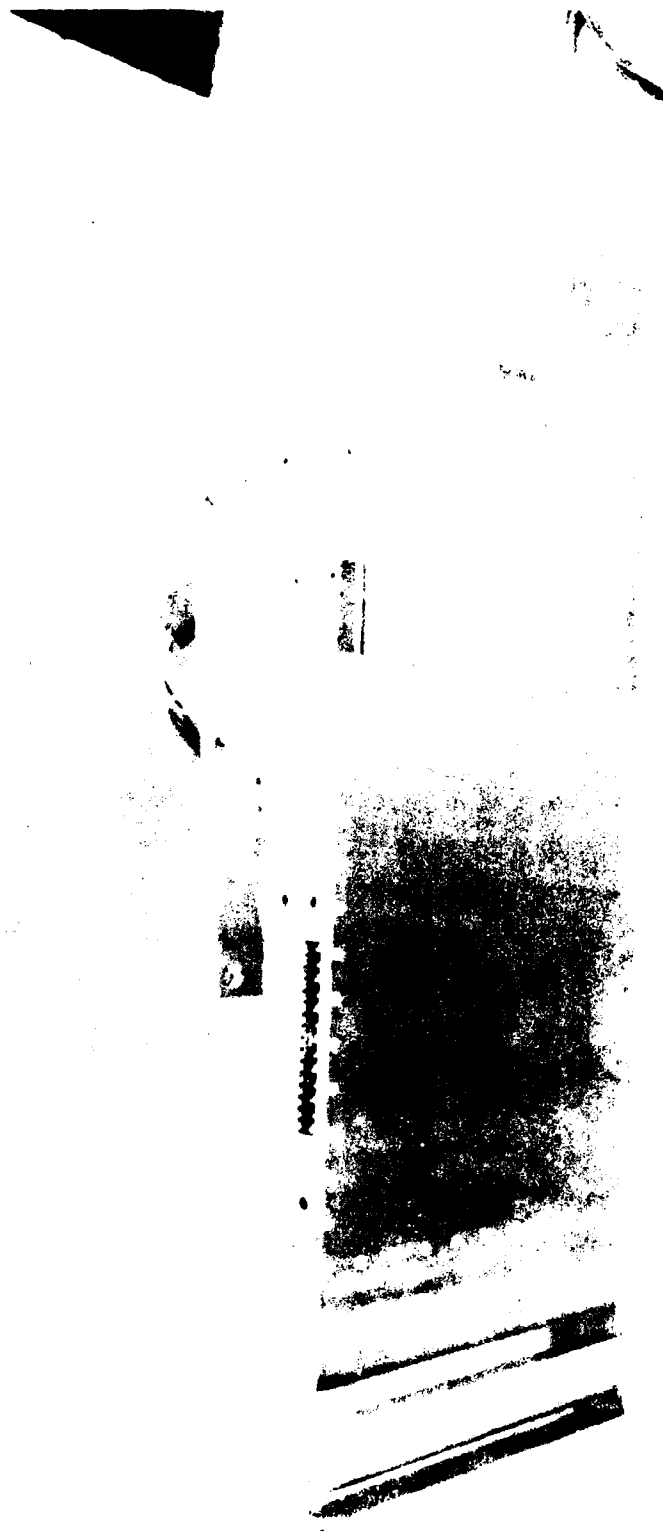
FIGURE 2. PHOTOGRAPH OF FLAT PLATE MODEL

5

a forward segment which was retracted before injection and extended during testing. After model injection into the tunnel, the model injection system (two pneumatic pistons driven by 100-300 psia air), shown in Figure 3, translated the forward plate section upstream and laterally into the plane of the stationary aft plate section. The forward section was designed to ride on pins in slots that guided it to either a retracted or extended position. Figures 4a and 4b show the model inside the tunnel in the collapsed and extended positions, respectively.

The stationary aft section of the model was mounted to a support pylon on the injection door. A pivot pin on the pylon allowed the model to be rotated to angles of attack up to 12 degrees (compression) relative to the flat plate surface. The pylon attachment was designed to keep the plate leading edge clear of the 7.28 in. thick tunnel wall boundary layer, and the trailing edge of the flap within the reflected bow shock of the sharp leading edge at 12 degrees angle of attack.

Design constraints were also placed upon the width of the model. First, it was necessary to keep the span edges of the plate clear of the tunnel wall boundary layer. The other opposing constraint was that the Mach lines from the extreme corners of the sharp leading edge not reach the extreme span corners of the flap trailing edge at a Mach number of 8, corresponding to 8 degrees angle of attack. The model width used, which was within the design constraints, was 15.0 in. The dimensions of the model in the extended position are shown in Figure 5. Two interchangeable primary surface plates and two interchangeable sets of flap surface plates were constructed. One set was instrumented with backface thermocouples and the other with pressure orifices and taps.

Heat transfer data were obtained from chromel-alumel thermocouples spot-welded to the backside of thin-skin (1/32 inch thick) sections obtained by counterboring 7/8 in. diameter flat bottomed holes in the primary 3/8 in. 15-4PH stainless steel plate. Thermocouple leads were welded with approximately 1/32 in. separation perpendicular to the mean flow direction. The flap plate thicknesses were a uniform 1/32 inch.

FIGURE 3. PHOTOGRAPH OF MODEL EXTENSION MECHANISM
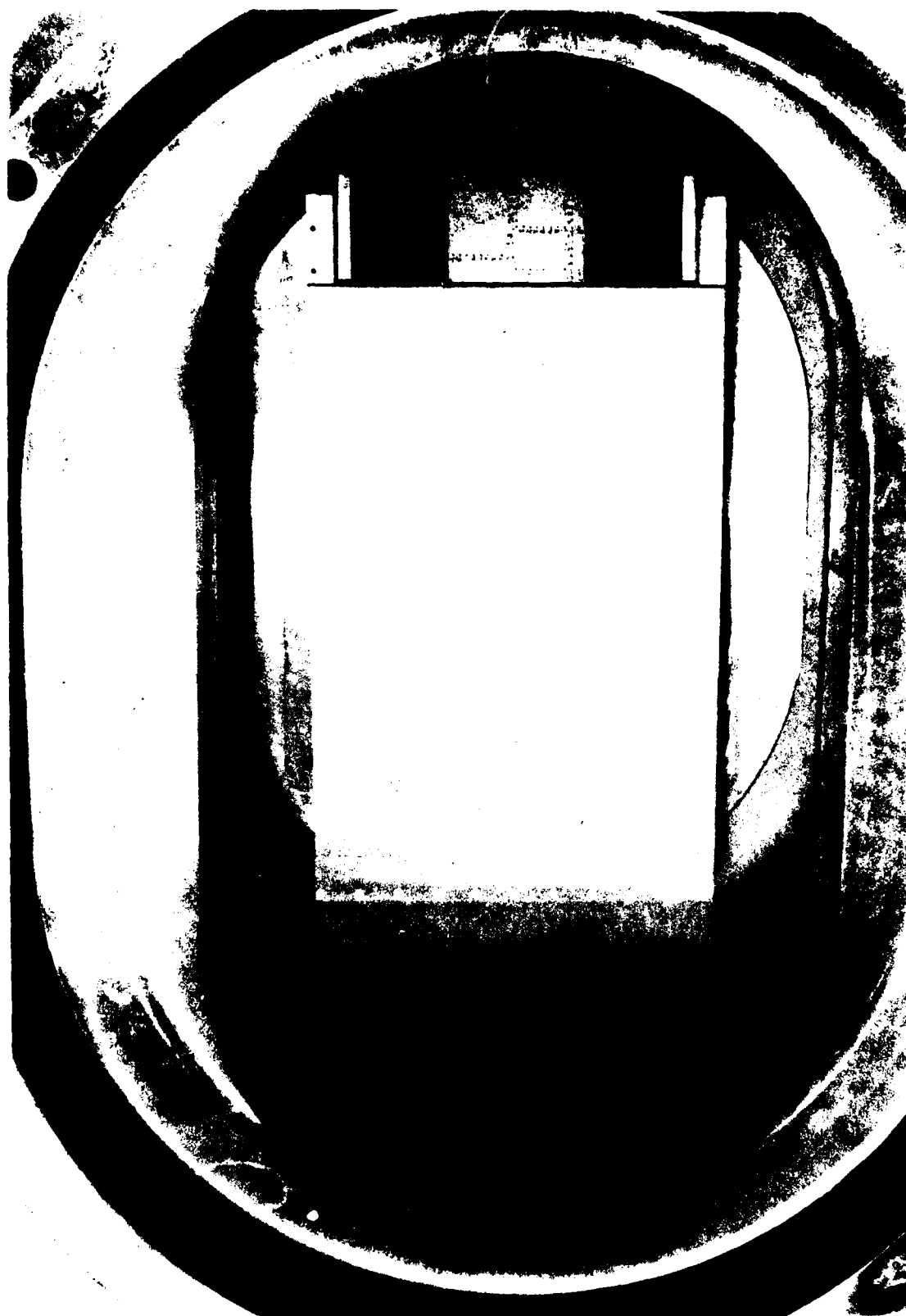
FIGURE 4a. PHOTOGRAPH OF MODEL IN LaRC CFHT IN RETRACTED POSITION

8

FIGURE 4b. PHOTOGRAPH OF MODEL IN LaRC CFHT IN EXTENDED POSITION

9

FIGURE 5. DIMENSIONS OF EXTENDABLE MODEL WITH 5 IN. SPAN FLAP
(SHOWN WITH PLATE'S THERMOCOUPLE LOCATIONS)

10

These flaps were essentially thin walled boxes with appropriate sliding joints for thermal expansion. Thermocouple data were taken over 2-5 second residence times in the flow.

Wall pressure measurements were made via orifices positioned on the plate and flaps. The pressure taps were .07 inch I.D. connected to piezoelectric transducers utilizing 5-foot long flexible tubing (.125 in. O.D.). Pressure tap locations were generally consistent with thermocouple locations; however, no pressure taps were located on the model's forward section due to the difficulty associated with extending the tubing.

In addition to the basic model discussed above, an instrumented flat plate model was mounted on the tunnel sidewall. This model was 12 in. wide and 24 in. long and so mounted as to form a 15 degree compression angle with the wall. Pressure tap and thermocouple locations for the sidewall model are illustrated in Figure 6.

FLOW DIRECTION
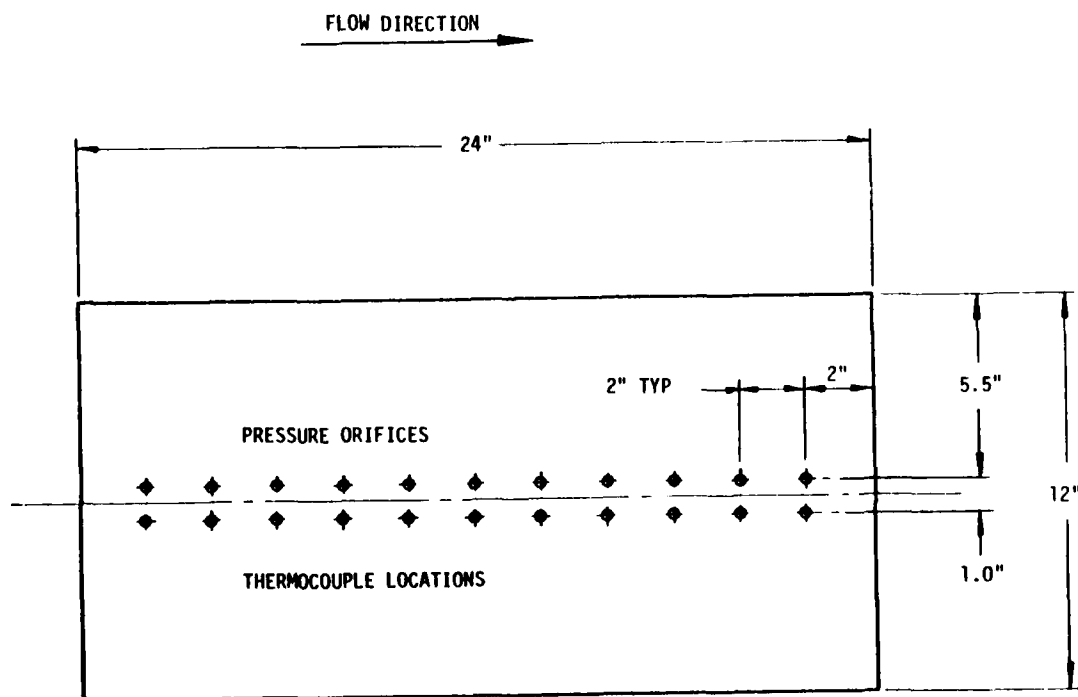
FIGURE 6. SIDEWALL MODEL DIMENSIONS

Finally, pitot pressure measurements of the boundary layer were obtained at the hinge line of the extendable flat plate model. Measurements were made with the 5 in. span flap at a zero degree deflection angle.

2.3 Data Reduction

The CFHT Heat Transfer Coefficient Program (Reference 2) was used to compute heat transfer rates from the measured temperature-time histories. This program computes heat transfer rates based upon the procedures of the thin skin, transient calorimeter technique. Digitized temperature-time data were obtained by sampling the thermocouple output at a rate of 20 times/second. From these measurements, a quadratic least squares curve fit of data over a one-second time interval was used to obtain $\partial T_w/\partial t$. With 0.0 seconds corresponding to model injection, the data over the interval 0.1 to 1.1 seconds were curve fit and the temperature derivative evaluated at the midpoint of the time interval. Upon obtaining $\partial T_w/\partial t$, the local heating rate was computed from

$$\dot{q} = \rho_{mm} l c_{mm} \, \partial T_w/\partial t \qquad (\text{BTU/ft}^2\text{-sec})$$

where ρ_{mm} and c_{mm} are model material density and specific heat and l is the local model thickness. Local radiative effects were ignored, as they were less than 1% of measured heating rates. Local heat transfer coefficients were then determined from

$$h = \frac{\dot{q}_{meas}}{\left(\dfrac{T_r}{T_t}\right) T_t - T_w}$$

where the specified value of the recovery-to-total temperature ratio, T_r/T_t, depended upon whether the flow was laminar or turbulent, and T_t was the measured freestream total temperature. Previous experience with similar instrumentation and this data reduction system has shown the reduced heat transfer data to be accurate to within 10 percent.

To support subsequent evaluations of the reduced data, the heat transfer coefficients were converted to non-dimensional Stanton number form by

$$St = \frac{h}{\rho_e u_e c_p}$$

where: ρ_e = edge density

                             u_e = edge velocity

                             c_p = specific heat (air), constant pressure

SECTION III

RESULTS AND DISCUSSION

Results obtained in the present experiment were evaluated to establish the basic reliability of the data and to characterize the pressure and heat transfer distributions on finite spans in turbulent boundary layer flows.

3.1 Heat Transfer Data Quality

The centerline distribution of measured Stanton numbers along the flat plate model surface (including the 5 in. span flap at zero degree deflection) at 12° angle of attack is shown in Figure 7. Data from two different tunnel runs are shown. In one of these runs, the aft facing step between the forward and aft plate sections was 30 mils, somewhat greater than the nominal limit of 10 mils. As is evident in Figure 7, the data are repeatable and the higher step (at station 25) has little influence on the downstream heating data. Fully turbulent flow, indicated by the maximum in the axial heating distribution, was obtained well ahead (10 boundary layer thicknesses) of the most forward edge of the flap.

In Figure 8, the measured centerline aeroheating distribution at 12 degrees angle of attack is compared to data obtained by Bertram and Neal (Reference 4) in the Ames 3.5 ft. tunnel at comparable test conditions. The present data are seen to be in general agreement with these previous measurements with some differences occurring in the location of transition onset. While the behavior of boundary layer transition indicated by these data is generally consistent with expected unit Reynolds number and leading edge thickness (bluntness) influences, achieving transition on the plate required a somewhat greater angle of attack (12 vs. 8 degrees) than suggested by the prior data. This effect is more clearly shown in Figure 9, where the 12 degree and 8 degree data are compared. The results demonstrate the need for the higher incidence angle to affect transition.
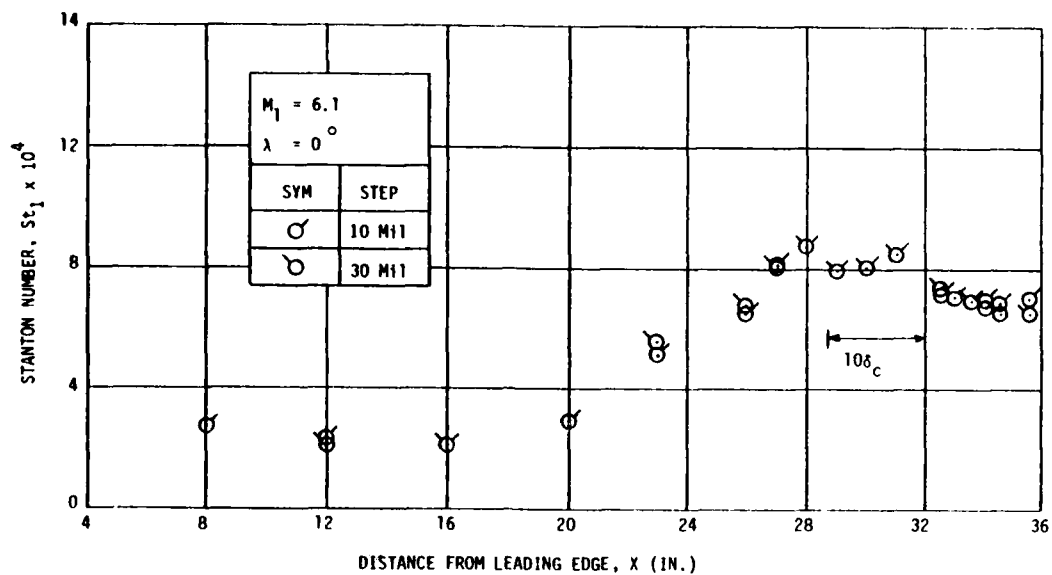
FIGURE 7. HEAT TRANSFER DATA CONSISTENCY
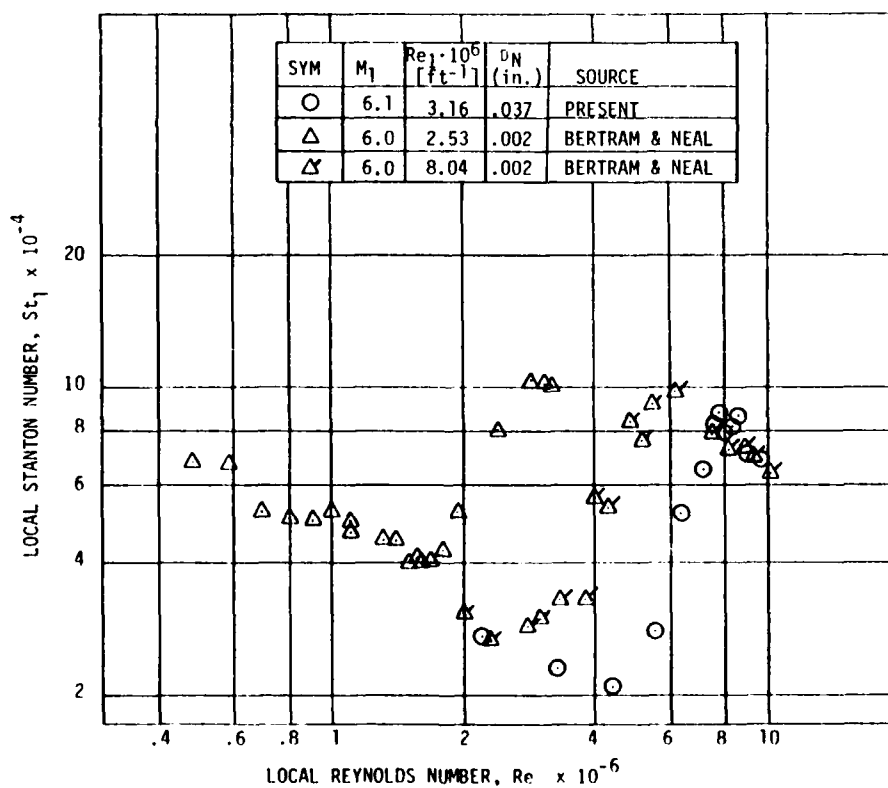
FIGURE 8. HEAT TRANSFER DATA VALIDITY

The comparison of the current heat transfer data to well-established theoretical predictions (Reference 5) is also shown in Figure 9. The agreement is good in both the laminar and turbulent regimes.

SYM	RUN	$\alpha°$	M_1	$Re_1 \cdot 10^6$
σ	15	12		
O	9	12	6.1	3.16
Δ	12	8		
Δ	7	8	7.4	3.39

VAN DRIEST (II)

$$St = \frac{.332}{\sqrt{Re_x}} \left(\frac{\rho^* \mu^*}{\rho \mu} \right)^{1/2} \frac{1}{(Pr)^{2/3}}$$

STANTON NUMBER, St

REYNOLDS NUMBER, Re_x

FIGURE 9. ANGLE OF ATTACK EFFECT ON BOUNDARY LAYER TRANSITION

3.1.1 Boundary Layer Transition

As noted above, a major problem in evaluating turbulent boundary layer viscous interaction phenomena in hypersonic flow ground test facilities is the establishment of the proper turbulent boundary layer characteristics. In this experiment, three tests were made to determine the condition of the boundary layer:

(1) Heat transfer rates upstream of the flap were
measured to detect the onset of turbulent
flow heating rates.

(2) The pitot pressure distribution normal to the
plate was measured to characterize the bound-
ary layer profile.

(3) Surface pressures upstream of the flap were
measured to detect boundary layer separation
if it occurred.

The design of the experiment was based on a combination of pre-
vious data from flat plate testing in the NASA CFHT (Reference 6) and data
reported by Pate in Reference 7. These prior data included observations
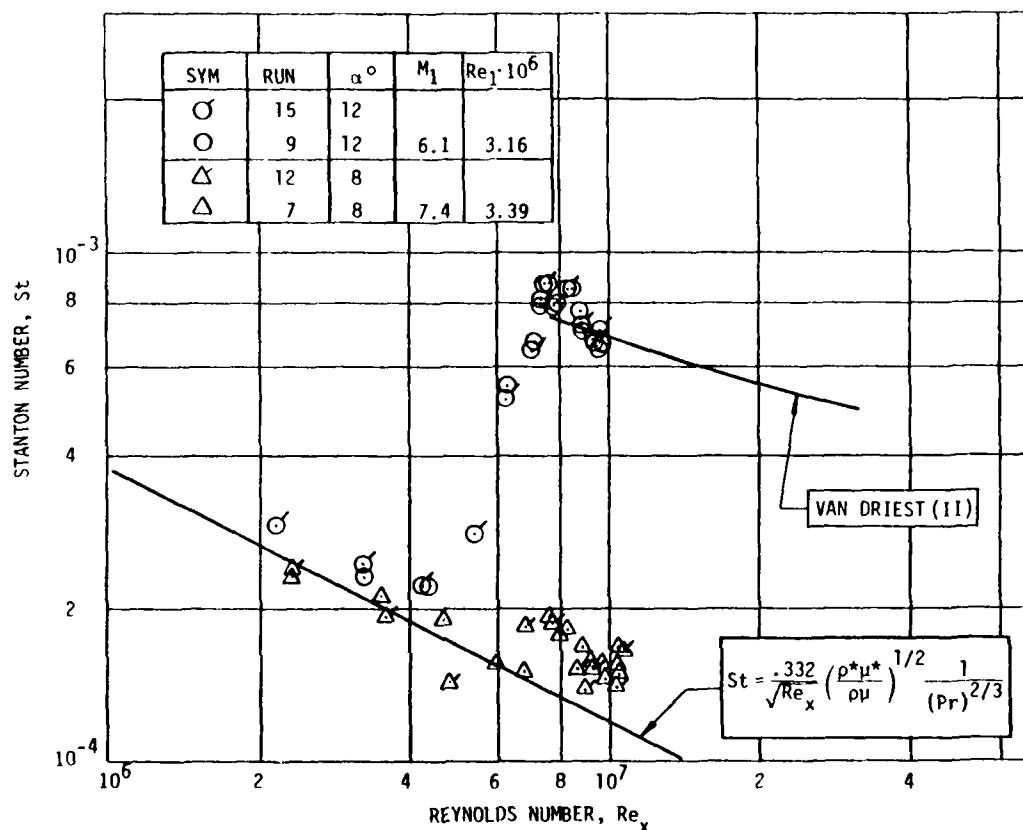of transition in the CFHT at lower unit Reynolds numbers (1.6×10^6/ft)
than that employed in the present test. The end of transition, therefore,
was expected to occur forward of the flap compression corner at 8 degrees
angle of attack. In the present experiment, not even transition onset was
observed on the plate at the 8 degree attitude, as illustrated previously
in Figure 9. The range of flat plate transition data from previous CFHT
experiments is illustrated in Figure 10.

The failure to duplicate previous boundary layer transition
observations at 8 degrees angle of attack caused some concern over the
validity of the results at 12 degrees angle of attack. Two possible
sources for the discrepancy are known. First, the unit Reynolds number
for the present experiment is significantly higher than that previously
achieved. The prediction of unit Reynolds number effect in the CHFT using
the Pate and Schueler correlation (Reference 8) is shown in Figure 10.
The second possible source of discrepancy is the larger leading edge
diameter employed in the present experiment than that used in previous
CFHT experiments. The leading edge diameter on the present model was
0.037 in., while that on the previously tested NASA LaRC model was 0.002
in. Linear extrapolation of the trend in transition Reynolds number with
bluntness Reynolds number, Re_D, reported by Potter and Whitfield in Ref-
erence 9 would indicate a shift of approximately 6×10^6 in $(Re_x)_t$. The
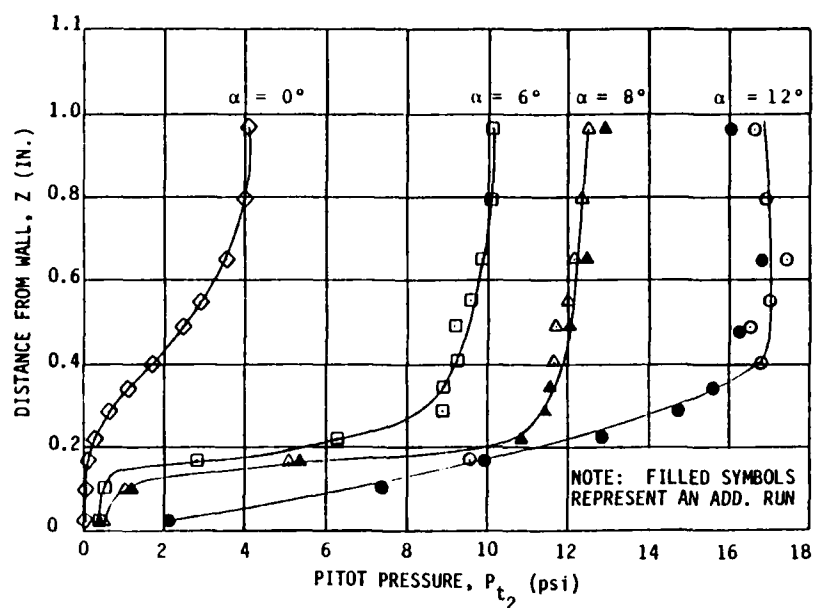
FIGURE 11.   PITOT RAKE MEASUREMENTS FOR SHARP NOSE FLAT PLATE

3.1.2 Boundary Layer Profiles

The pitot pressure distributions were measured in the boundary layer at the location of the compression corner, for a zero degree flap deflection. Presented in Figure 12 is the nondimensionalized pitot pressure profile for the 12 degree data. The static pressure measured at this location was .335 psia which agrees very closely with the value predicted by the oblique shock relations. Assuming the static pressure to be constant through the boundary layer, the Mach number distribution can be determined from the isentropic flow equations. The Crocco-Busemann equation (Reference 10), modified for Prandtl number not equal to 1,

$$\frac{T}{T_e} = \frac{T_w}{T_e} + \left(\frac{T_r}{T_e} - \frac{T_w}{T_e}\right)\frac{u}{u_e} + \left(1 - \frac{T_r}{T_e}\right)\left(\frac{u}{u_e}\right)^2 \tag{1}$$

can then be used with the computed Mach number profile

$$\frac{M}{M_e} = \frac{u}{u_e}\sqrt{\frac{T_e}{T}} \tag{2}$$

19

to calculate the boundary layer velocity profile. These velocity/position
points (except the point next to the wall where wall interference is
likely present) have been transformed to logarithmic coordinates in Figure
13. The slope of a linear fairing through these points yields the exponent
of the power law velocity profile

$$\frac{u}{u_e} = \left(\frac{y}{\delta_c}\right)^{1/11.4} \tag{3}$$

where the boundary layer thickness at the compression corner, δ_c, is 0.31
in.
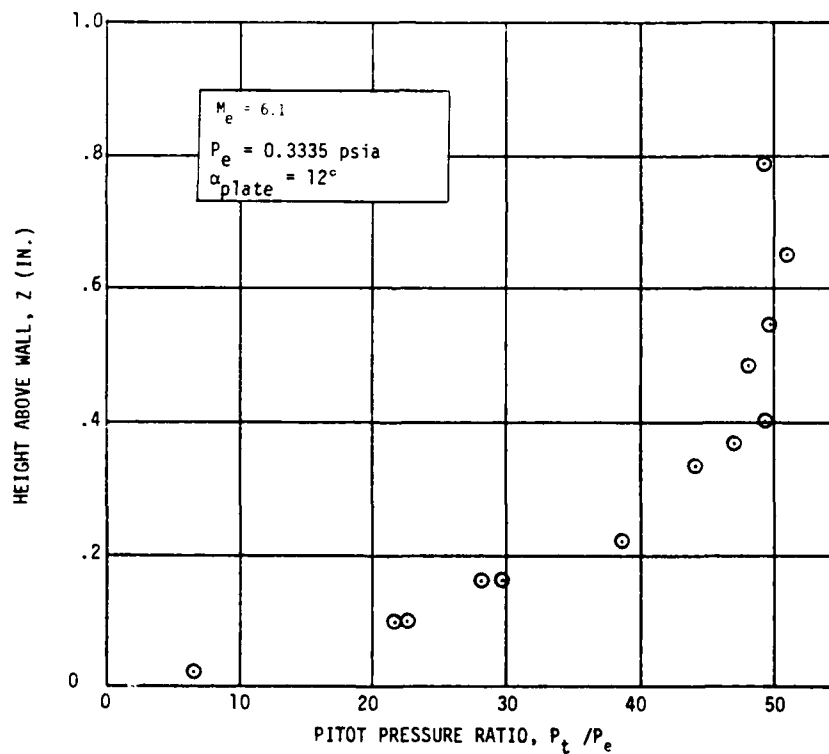
FIGURE 12.   PITOT PRESSURE SURVEY FOR TURBULENT BOUNDARY LAYER

$\delta_c = 0.31$ in.
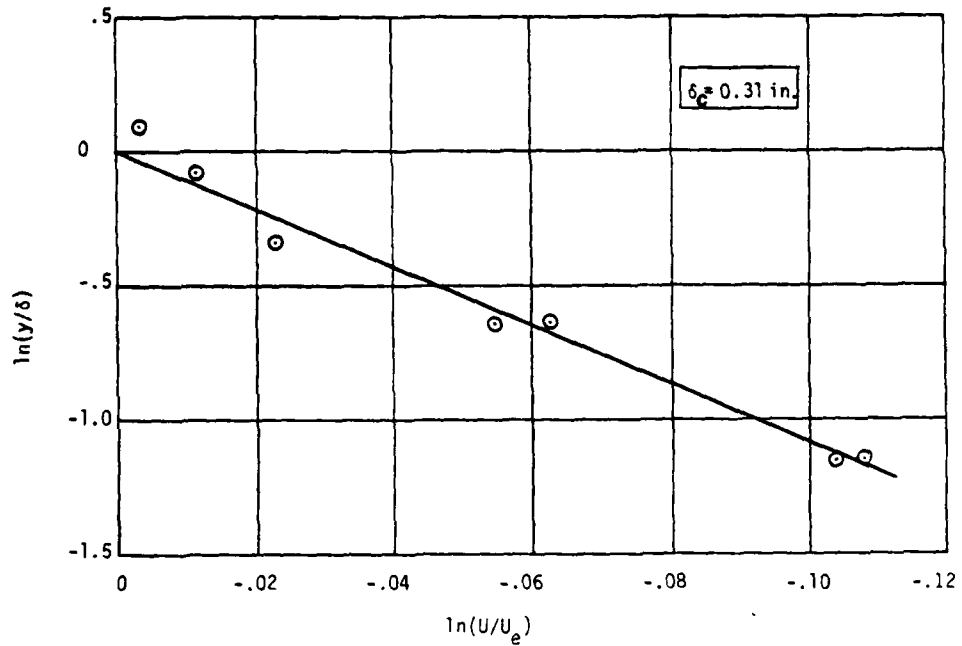
FIGURE 13.   VELOCITY PROFILE IN TURBULENT BOUNDARY LAYER AT STATION 32

Following the method employed by Hopkins, Keener and Dwyer in Reference 11, the velocity distribution in the boundary layer has been transformed to the incompressible equivalent reduced velocity profile by the van Driest (Reference 5) function

$$\frac{\bar{u}}{u_\tau} = \frac{1}{A\left[\frac{1}{2}C_{f_e}T_w/T_e\right]^{\frac{1}{2}}} \left\{ \sin^{-1}\left[\frac{2A^2 u/u_e - B}{(4A^2 + B^2)^{\frac{1}{2}}}\right] + \sin^{-1}\left[\frac{B}{(4A^2 + B^2)^{\frac{1}{2}}}\right] \right\} \quad (4)$$

where: $A = \left(0.2\, M_e^2\, \frac{T_e}{T_w}\right)^{\frac{1}{2}}$, $B = \frac{T_e}{T_w} + A^2 - 1.$

21

This distribution is compared in Figure 14 to the transformed data of Hopkins, Keener and Dwyer. Also shown is Cole's law of the wall and wake (Reference 12) in the form

$$\frac{\bar{u}}{u_\tau} = \frac{1}{K} \ln\left(\frac{u_\tau y}{\nu_w}\right) + C + \frac{1}{K}\pi\omega \tag{5}$$

where: $K = 0.41$, $C = 5.0$

$$\pi = 0.55 \left\{ 1 - \exp\left[-0.243\sqrt{\frac{Re_\theta}{425} - 1} \quad -0.298\left(\frac{Re_\theta}{425} - 1\right)\right]\right\}$$

Re_θ = momentum thickness Reynolds number

$$u_\tau = \sqrt{\frac{\tau_w}{(\rho_w/g)}}$$

$$\omega = 2 \sin^2\left[(\pi/2)(y/\delta)\right]$$

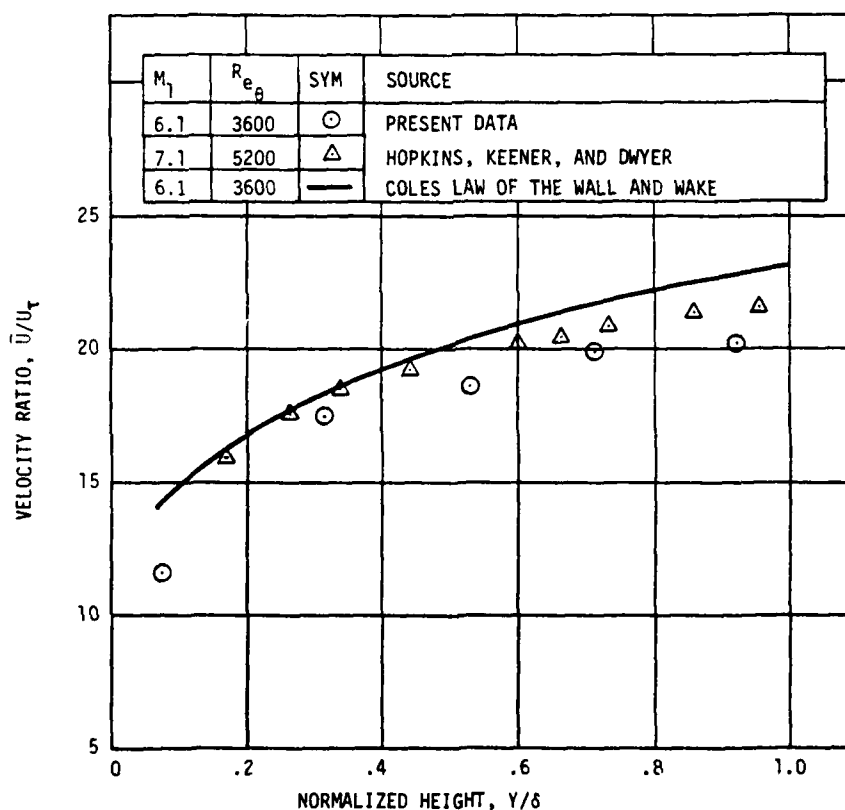| M_1	Re_θ	SYM	SOURCE
6.1	3600	⊙	PRESENT DATA
7.1	5200	△	HOPKINS, KEENER, AND DWYER
6.1	3600	——	COLES LAW OF THE WALL AND WAKE

FIGURE 14.   TRANSFORMED VELOCITY PROFILES

22

The results presented in Figures 11-14 indicate that the boundary layer approaching the flap in the present experiment was turbulent. Since the exponent of the power law velocity profile (~1/11) had not attained the value indicative of equilibrium turbulence (~1/7), it appears that the approaching boundary layer was in a state of non-equilibrium turbulence.

3.1.3 Two-Dimensionality of Approaching Flow

The spanwise distribution of pressures at station 29 on the plate is illustrated in Figure 15. The Stanton number distribution at the same station is illustrated in Figure 16. Although the spanwise pressure distribution on the plate is influenced by edge effects, the pressure along the leading edge of the widest span flap is characteristic of two-dimensional flow. However, the heating data seem to indicate a peak heating off the centerline. This may be due to the fact that the centerline heat transfer result at station 29 is a low measurement as indicated by the trend of the centerline heat transfer data shown in Figure 7.
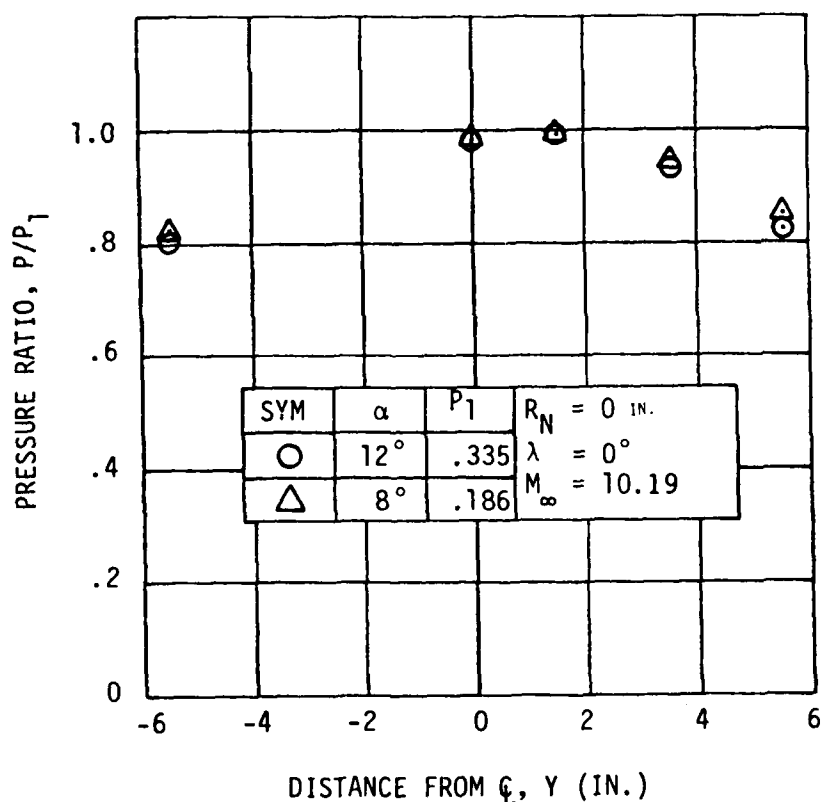

FIGURE 15. LATERAL PRESSURE DISTRIBUTION ON THE PLATE AT STATION 29
(3 IN. UPSTREAM OF COMPRESSION CORNER)

23
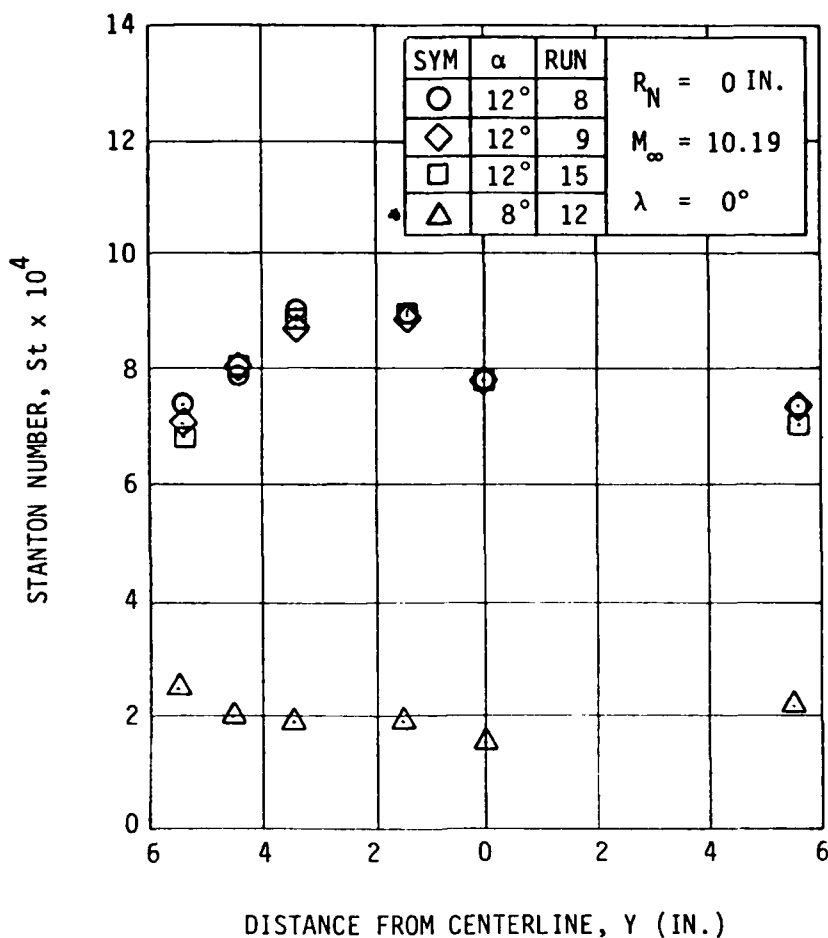
FIGURE 16.   LATERAL HEATING DISTRIBUTION OVER PLATE AT STATION 29
(3 IN. UPSTREAM OF COMPRESSION CORNER)

Surface pressure and heat transfer measurements on the NASA LaRC
CFHT sidewall plate, on which the sidewall flap was mounted as part of the
present experiment, were reported by Throckmorton in Reference 13. The
data are not shown here, but Throckmorton reports that a significant
lateral flow exists in the CFHT sidewall boundary layer. Although it was
realized that the lateral flow effects would seriously complicate the re-
duction and interpretation of the sidewall flap data, it was anticipated

that at least qualitative information could be obtained which would demonstrate the effect of a thick turbulent boundary layer on flap performance.

3.2 Flap Centerline Flow Properties

⌐· ⌐ed pressure and heat transfer distributions along the flap centerline ∟ ⌐ar to be consistent with distributions measured on nearly two-dimensional flaps by other investigators. The spanwise pressure and heat transfer distributions were constant over a significant fraction of the widest span flap, as will be shown below.

3.2.1 Measured Centerline Flow Properties

The behavior of pressure and/or heat transfer distribution along the centerline chords of compression flaps with effectively infinite spans has been reported by Roshko and Thomke (Reference 14), Holden (References 17 and 18), Elfstrom (References 15 and 19), and Coleman and Stollery (Reference 16). Although the investigations were primarily directed toward the case of incipient separation, they also provide valuable data and insights for the attached flow case, usually at high deflection angles. The flap deflection angles maintained in the present experiment (0 to 15 degrees) were below the value required for separation. The distribution of pressure coefficient, $(C_p)_1$, along the 5 in. flap used in the present experiment is shown in Figure 17 for each of four deflection angles. Note that boundary layer separation was not evidenced, as all the pressure values at a point 1 in. upstream of the compression corner are coincident, regardless of the deflection angle.

Centerline pressure data, obtained in the present experiment and in previous investigations, for a 15 degree ramp under a variety of upstream conditions are shown in Figure 18. An appropriate length scale for the pressure distributions is the oncoming boundary layer thickness, as demonstrated in Figure 18. With the exception of the sidewall data, for which the flap chord was only three boundary layer thicknesses in length, the pressure distributions approach their respective inviscid wedge values approximately 5 to 6 boundary layer thicknesses downstream of the compression corner. It would thus seem appropriate to scale the ordinate
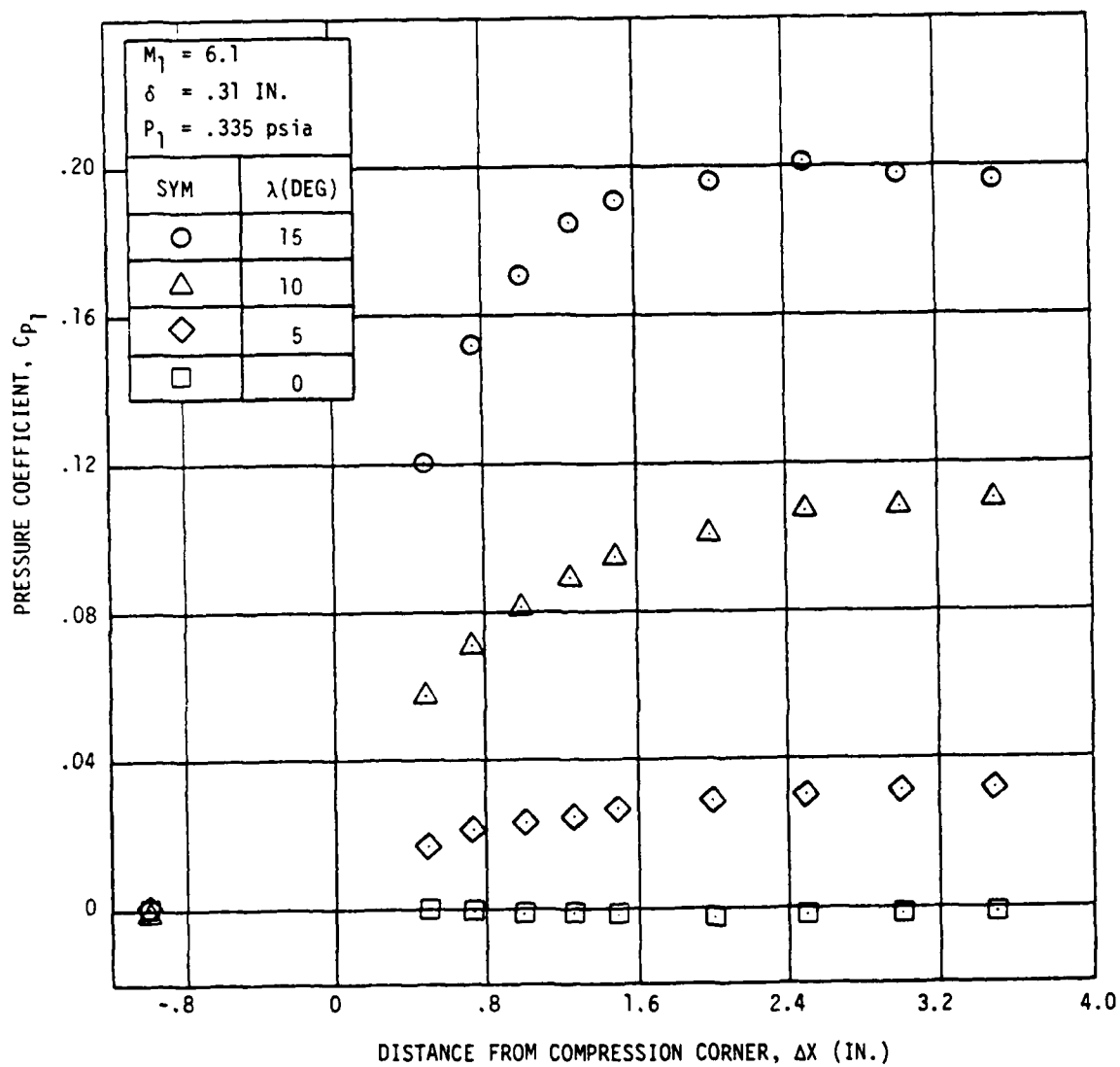
25

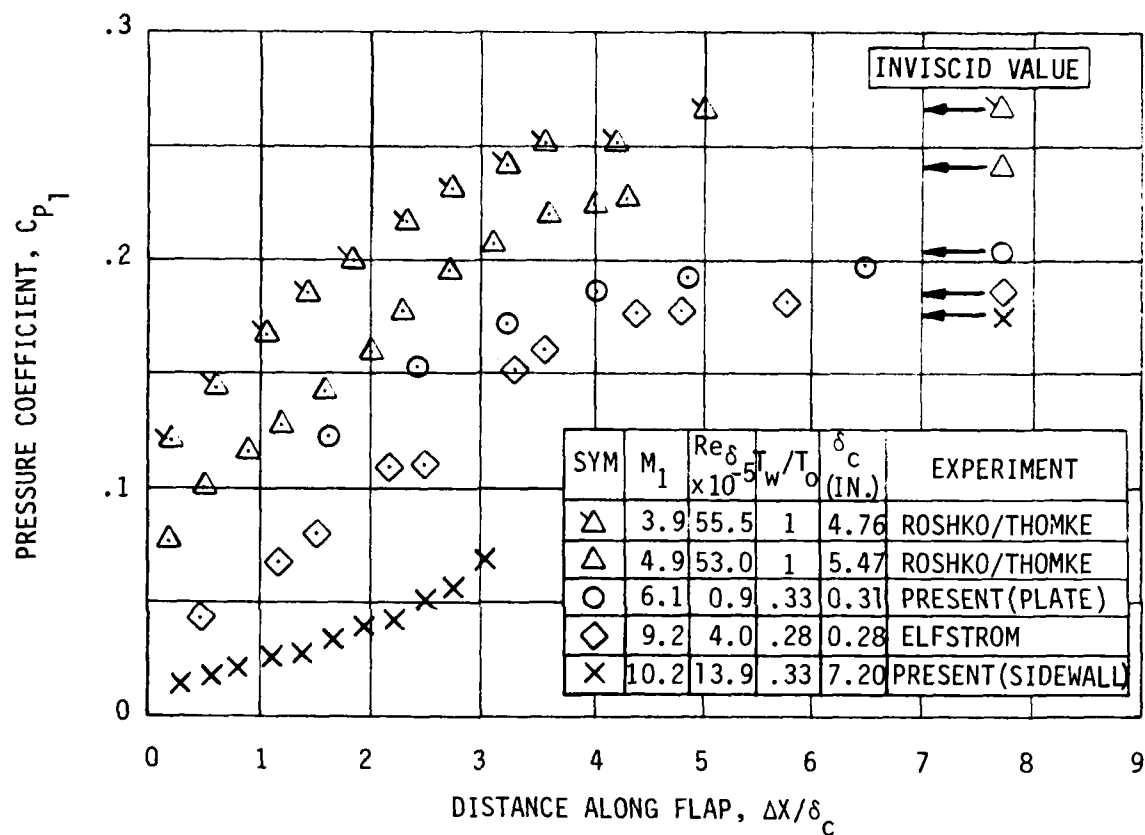FIGURE 17. FLAP CENTERLINE PRESSURE DISTRIBUTION FOR 5 IN. SPAN FLAP

FIGURE 18. FLAP CENTERLINE PRESSURE DISTRIBUTION COMPARISONS (15° COMPRESSION ANGLE)

The figure shows PRESSURE COEFFICIENT, c_{P_1} versus DISTANCE ALONG FLAP, $\Delta X/\delta_c$, with an INVISCID VALUE legend and the following table:

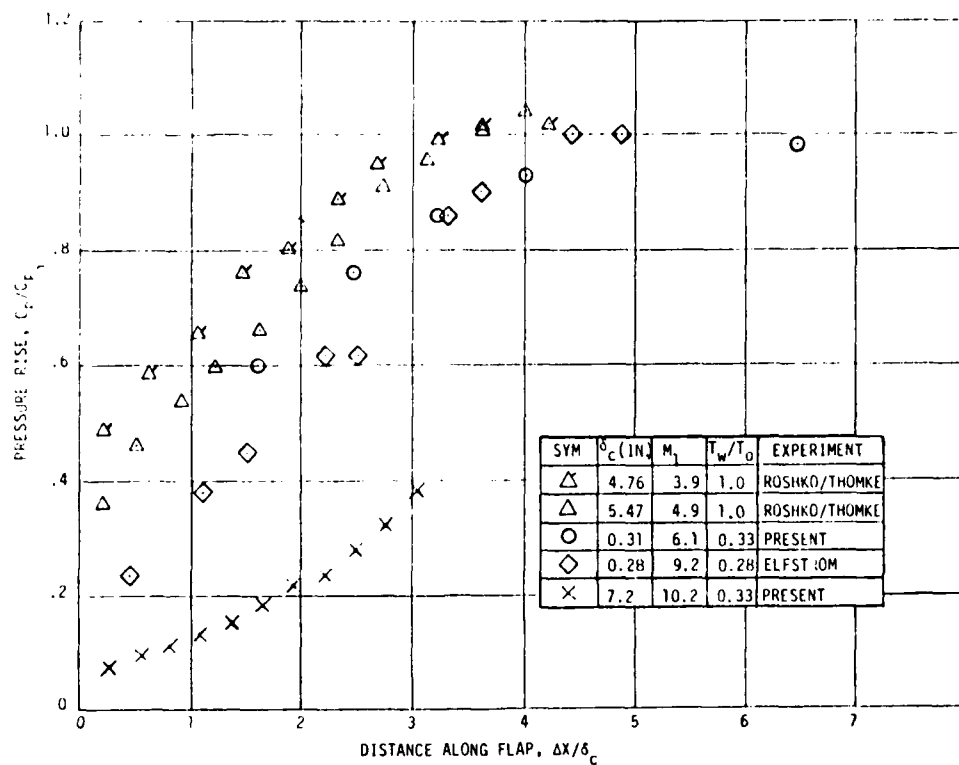| SYM	M_1	$Re_\delta \times 10^{-5}$	T_w/T_o	δ_c (IN.)	EXPERIMENT
△	3.9	55.5	1	4.76	ROSHKO/THOMKE
△	4.9	53.0	1	5.47	ROSHKO/THOMKE
O	6.1	0.9	.33	0.31	PRESENT(PLATE)
◇	9.2	4.0	.28	0.28	ELFSTROM
X	10.2	13.9	.33	7.20	PRESENT(SIDEWALL)

27

FIGURE 19. FLAP PRESSURE RISE SCALING AT A 15 DEGREE COMPRESSION CORNER

with $(C_p)_i$. As shown in Figure 19 the distributions are reduced to a
family of curves with the Mach number as an apparent parameter. Conditions
upstream of the CFHT sidewall flap (M_1 = 10.2 in Figure 19) were known to
deviate from a two-dimensional, zero pressure gradient flow, and the
sidewall flap pressure data do not follow the trend of the other data. A
simple empirical correlation which fits the data in Figure 19 reasonably
well for $\Delta X/\delta_c$ < 7 is

$$\frac{Cp}{Cp_i} = m_1 + m_2\left(\frac{\Delta X}{\delta_c}\right) + m_3\left(\frac{\Delta X}{\delta_c}\right)^2 \tag{6}$$

where: $m_1 = 0.65 - 0.058M_1$

$m_2 = 0.099 + 0.017M_1$

$m_3 = -0.0071 - 0.0012M_1$

It is assumed that the pressure coefficient attains the inviscid level and
remains constant for $\Delta X/\delta_c$ < 7. Although this fit was extracted from
pressure data taken for 15 degree flaps, the equation is in general agree-
ment with the 10 degree data of the present experiment.

The distributions of measured centerline heating rates on the
widest span flap are shown in Figure 20 for deflection angles of 0, 5, 10
and 15 degrees. The data are expressed in terms of the nondimensional
Stanton number, St_1, where the subscript 1 signifies that the quantity is
referenced to conditions immediately upstream of the flap. The heat
transfer distribution for the sidewall ramp (λ = 15 degrees) is shown in
Figure 21. For comparison, the data reported by Coleman and Stollery in
Reference 16 for a flap subjected to approximately the same upstream Mach
number are also shown in Figure 21. The Coleman and Stollery data were
taken for the same thin oncoming boundary layer as were the pressure data
reported by Elfstrom in Reference 15 (Figures 18 and 19). As will be
shown in the section below, the shape of the oncoming Mach number profile
has a significant effect on the distribution of surface pressure and heat

transfer along the flap centerline. The data in Figure 21 possibly support this finding since the upstream Mach number profiles were not similar. A simple scaling of the heat transfer data by the approaching boundary layer thickness is, in this case, inadequate.
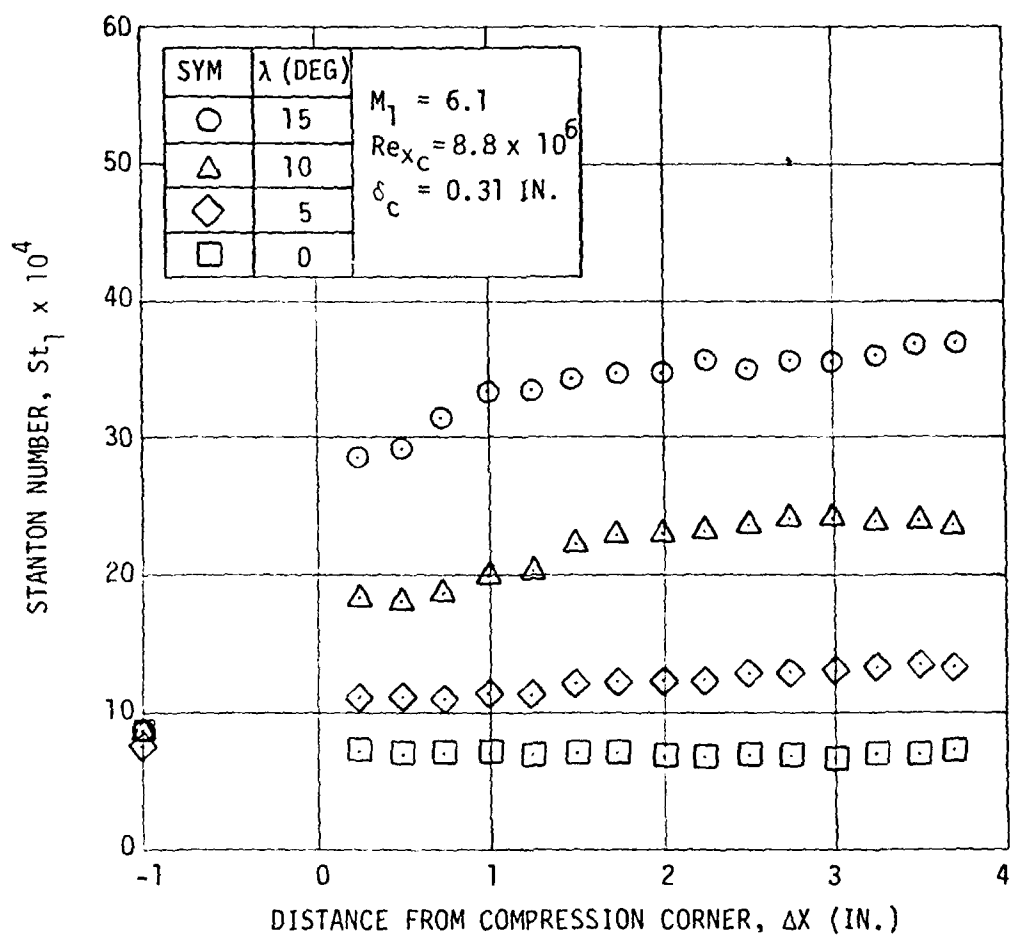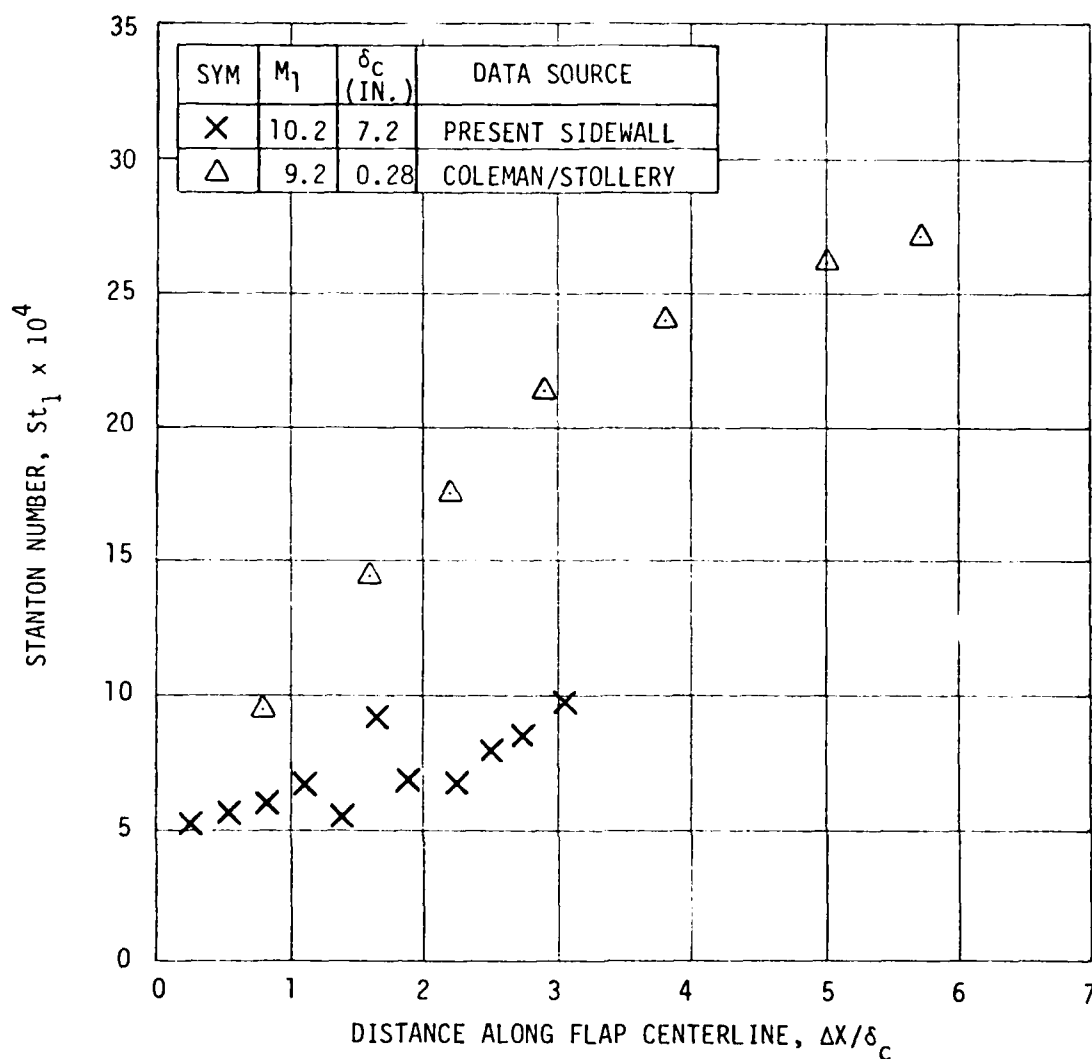

FIGURE 20. FLAP CENTERLINE HEAT TRANSFER DISTRIBUTION

FIGURE 21. SIDEWALL RAMP HEAT TRANSFER DISTRIBUTION

3.2.2 Prediction of Centerline Flow Properties

Previous investigators have provided some insight into the nature of the attached flow compression interaction on effectively two-dimensional flaps. Elfstrom (Reference 15) reports that Schlieren photographs show the flap shock penetrating deep into the boundary layer,

indicating a thin subsonic region. Elfstrom also demonstrates that neither Reynolds number nor wall temperature has any significant effect on the centerline pressure distribution. Roshko and Thomke (Reference 14) made similar observations and modeled the attached flow compression as an inviscid, rotational flow. A method of characteristics was used to predict the static pressure distribution along the wedge.

Elfstrom later followed a similar approach but alleviated much of the complexity associated with the method of characteristics. The Mach number profile upstream of the flap is divided into layers of constant Mach numbers, as shown in Figure 22a. The layer adjacent to the wall is assumed to be supersonic. Starting with the lowest layer, the curved shock is constructed layer-by-layer using the local upstream Mach number and the wedge angle to obtain the local shock angle. The entire flowfield behind the shock is assumed to turn parallel to the flap. Given the Mach number distribution behind the shock, the Mach lines may be traced from the shock to the flap surface. It is assumed that the pressure disturbances propagate along the Mach lines and do not reflect.

An even simpler approach is illustrated in Figure 22b. Mach numbers behind the shock are computed using the wedge angle and the local upstream Mach number. However, the Mach lines are assumed to extend from a straight shock whose angle is determined from the edge Mach number and the wedge angle. Furthermore, the angles of the Mach lines immediately behind the shock are assumed to travel to the flap surface in a straight line. In this manner, a closed-form expression may be derived which provides the relationship between the height, Y, of a Mach number, $M_1(Y)$, in the approaching flow and the corresponding location, ΔX, of the corresponding pressure rise on the flap,

$$\frac{\Delta X}{Y} = \frac{1}{\sin \beta} \left[\cos (\beta - \lambda) + \frac{\sin(\beta - \lambda)}{\tan \mu_2} \right] \tag{7}$$

where β is the shock angle at the boundary layer edge and μ_2 is the local Mach angle behind the shock. Although this simplified method has no firm physical basis, it agrees reasonably well with Elfstrom's method and with available data, as will be shown.
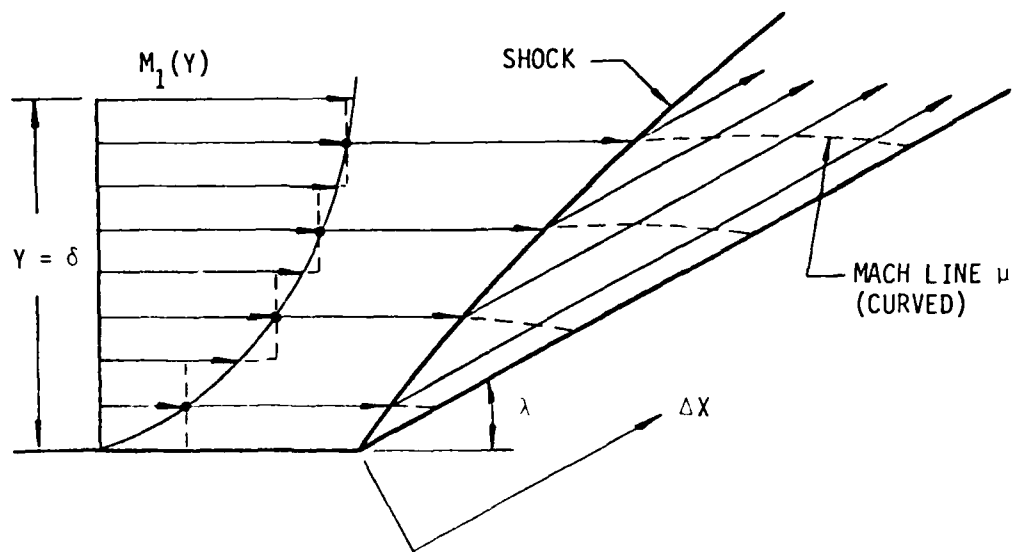
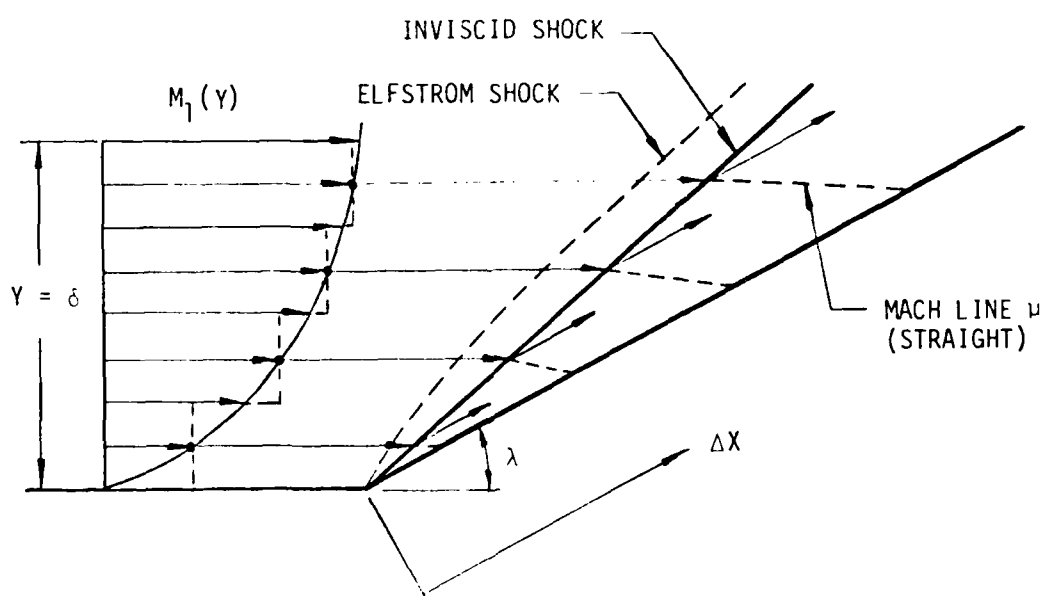FIGURE 22a. ELFSTROM FLOW MODEL

FIGURE 22b. SIMPLIFIED FLOW MODEL

33

A method for predicting centerline heat transfer distributions on the flap was proposed by Coleman and Stollery (Reference 16)

$$\frac{\dot{q}_{\Delta X}}{\dot{q}_c} \doteq \left[\frac{\rho_2 u_2}{\rho_1 u_1}\right]_y \left[\frac{M_1}{M_2}\right]_y^{1.3} \tag{8}$$

where $\dot{q}_c$ is the heat transfer rate immediately upstream of the compression corner. They demonstrate that this approximation, combined with the method suggested with Elfstrom, provides good agreement with measurements they made as well as with Holden's measurements (Reference 17).

Comparisons of the modified Elfstrom method, for predicting flap surface pressures, and the Coleman and Stollery method, for predicting flap centerline heat transfer rates, with available data are presented in Figures 23-26 for deflection angles of 5, 10, 15 and 30 degrees, respectively. Equation (7) was used to construct the curves relating $\Delta X/Y$ to $M_1 (Y/\delta_c)$. Such curves are independent of the shape of the Mach number profile. With the exception of the Mach number profile upstream of the sidewall flap, the Mach number profiles for the various data are similar, as shown in Figure 27. The modified Elfstrom method compares well with the pressure data presented. The Coleman and Stollery method, used in conjunction with the modified Elfstrom method (equation 7), compares reasonably well with the heat transfer data. However, for the 15 degree deflection, the method shows good agreement only with Coleman and Stollery's data.

3.3 Finite Span Effects on Pressure and Heat Transfer

A primary objective of the experiments conducted under this program was to evaluate the influence of finite flap spans on pressure and heating levels on the flap surface, with a specific orientation toward design applications. The bulk of the earlier work in this area, in contrast, was focused principally on the separation problem and the detailed physics of the separation process. Gray and Rhudy (Reference 21) did, however, previously examine some finite span effects for the attached flow situation.
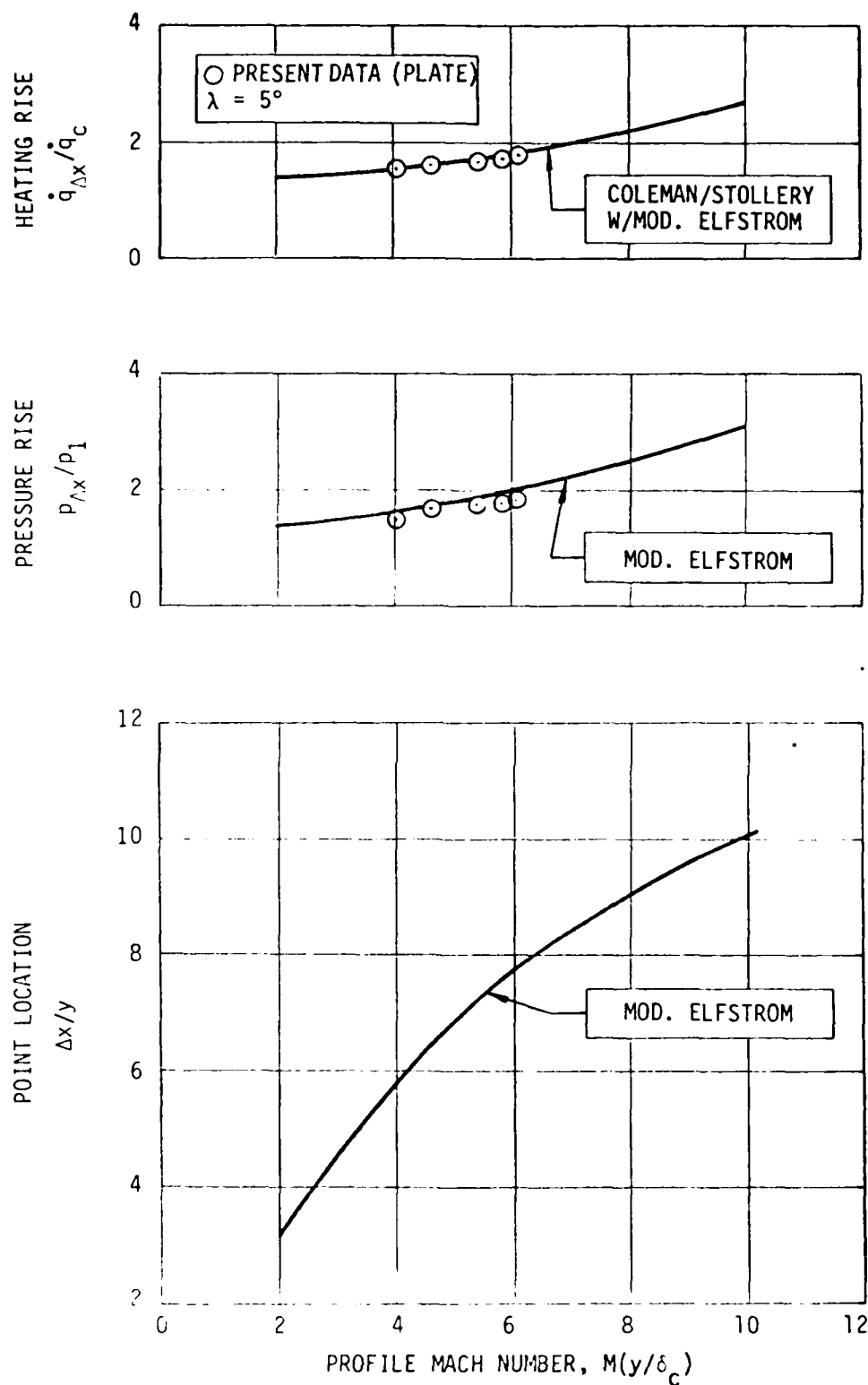
FIGURE 23. COMPARISON OF FLAP DATA WITH ELFSTROM AND COLEMAN/
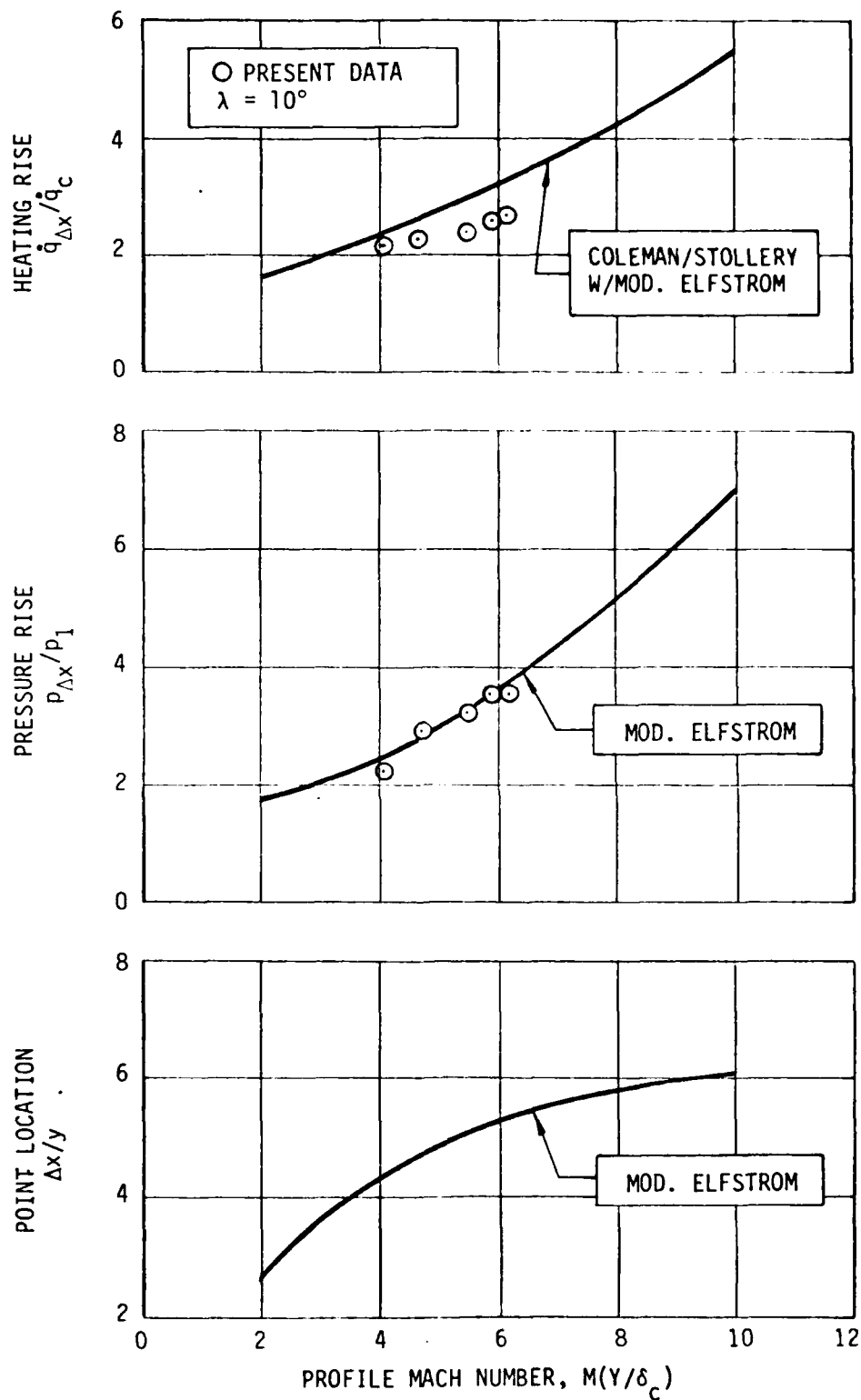STOLLERY PREDICTION AT 5° COMPRESSION ANGLE

FIGURE 24. COMPARISON OF FLAP DATA WITH ELFSTROM AND COLEMAN/
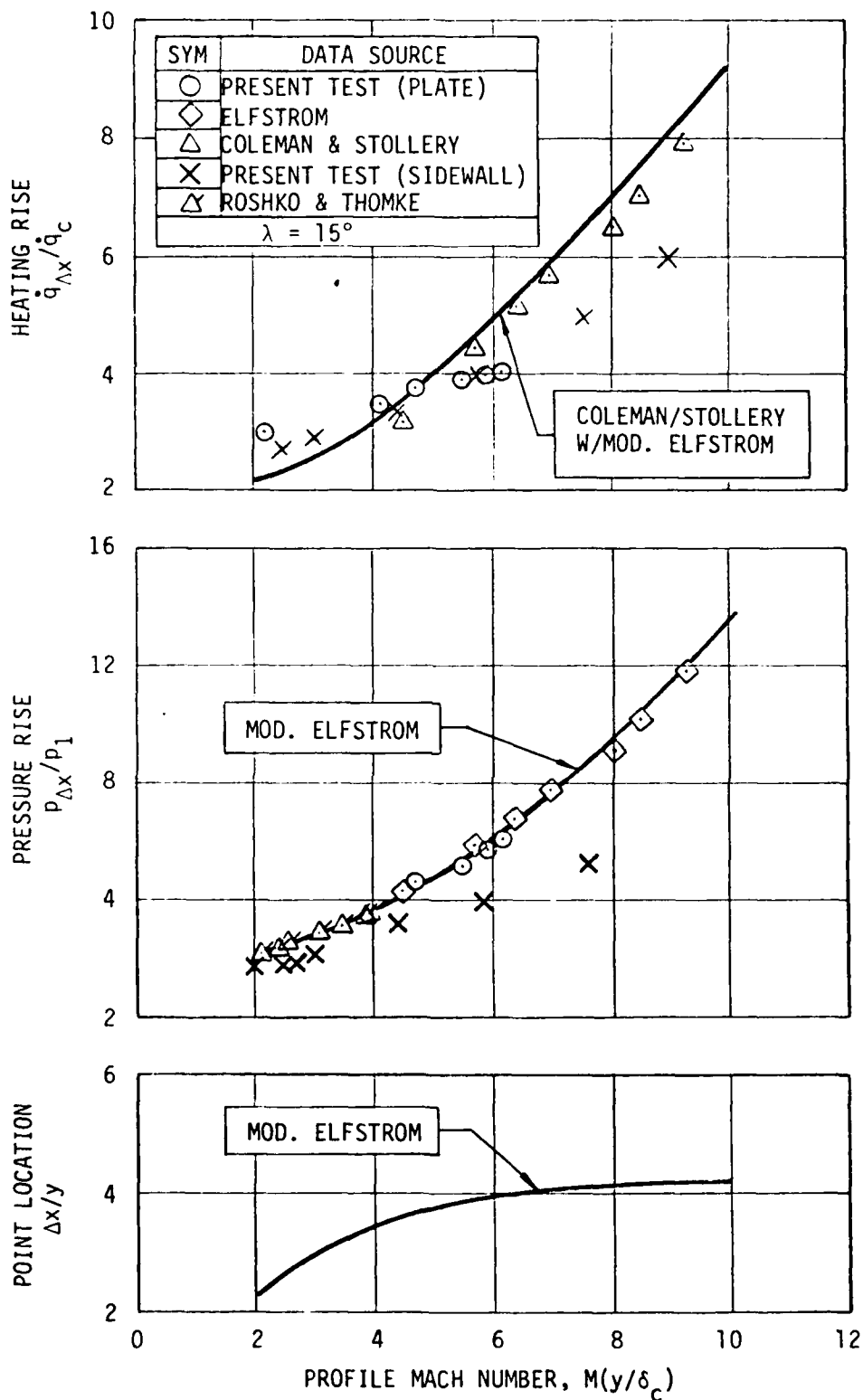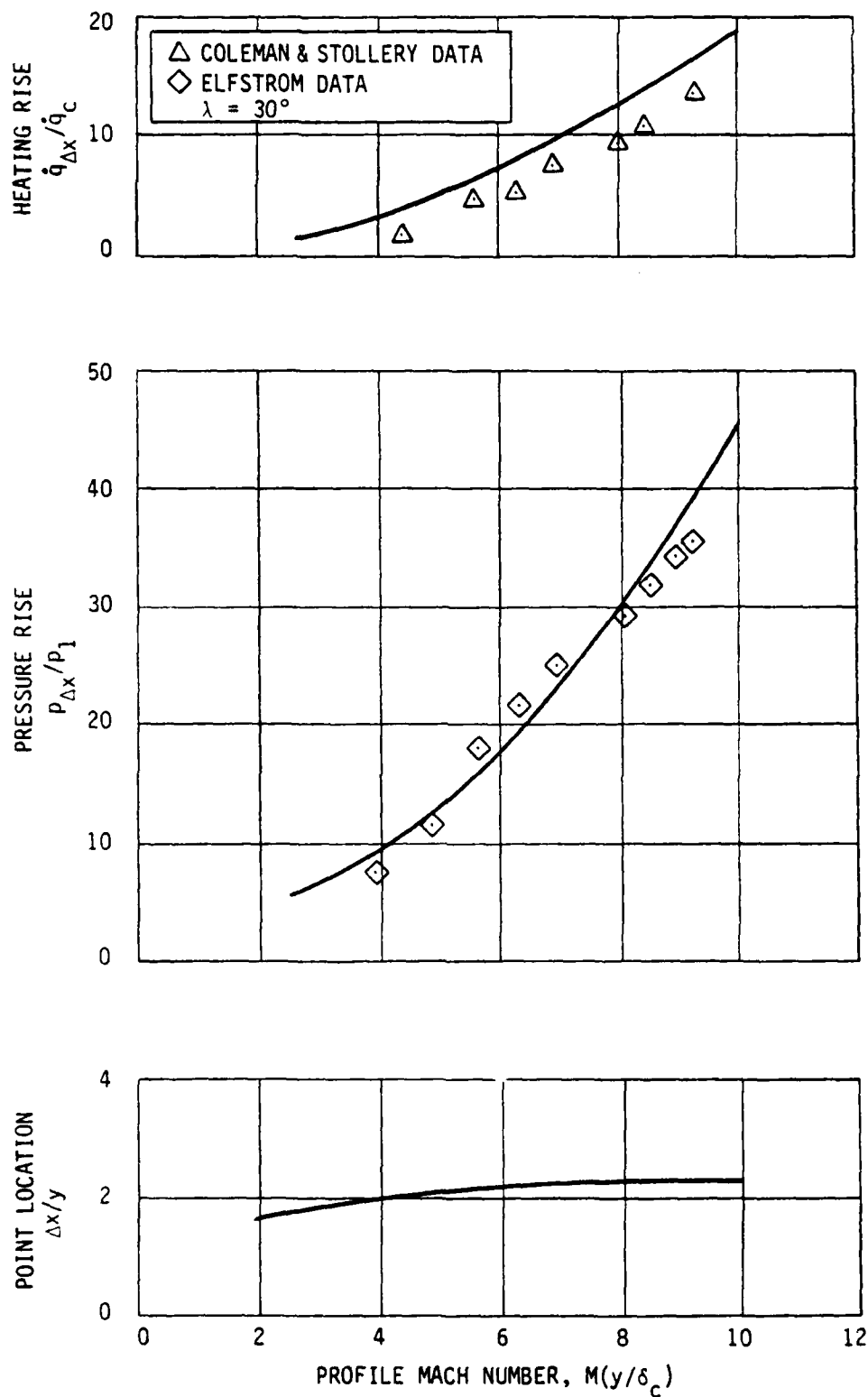STOLLERY PREDICTION AT 10° COMPRESSION ANGLE

36

FIGURE 25. COMPARISON OF FLAP DATA WITH ELFSTROM AND COLEMAN/
STOLLERY PREDICTION AT 15° COMPRESSION ANGLE

FIGURE 26. COMPARISON OF FLAP DATA WITH ELFSTROM AND COLEMAN/
STOLLERY PREDICTION AT 30° COMPRESSION ANGLE

38

illustrated in Figure 28. The Mach number downstream of the flap shock, in the flow just outside the boundary layer, is termed M_{2_e}, with the associated Mach line given by $\mu_2 = \sin^{-1}(1/M_{2_e})$.
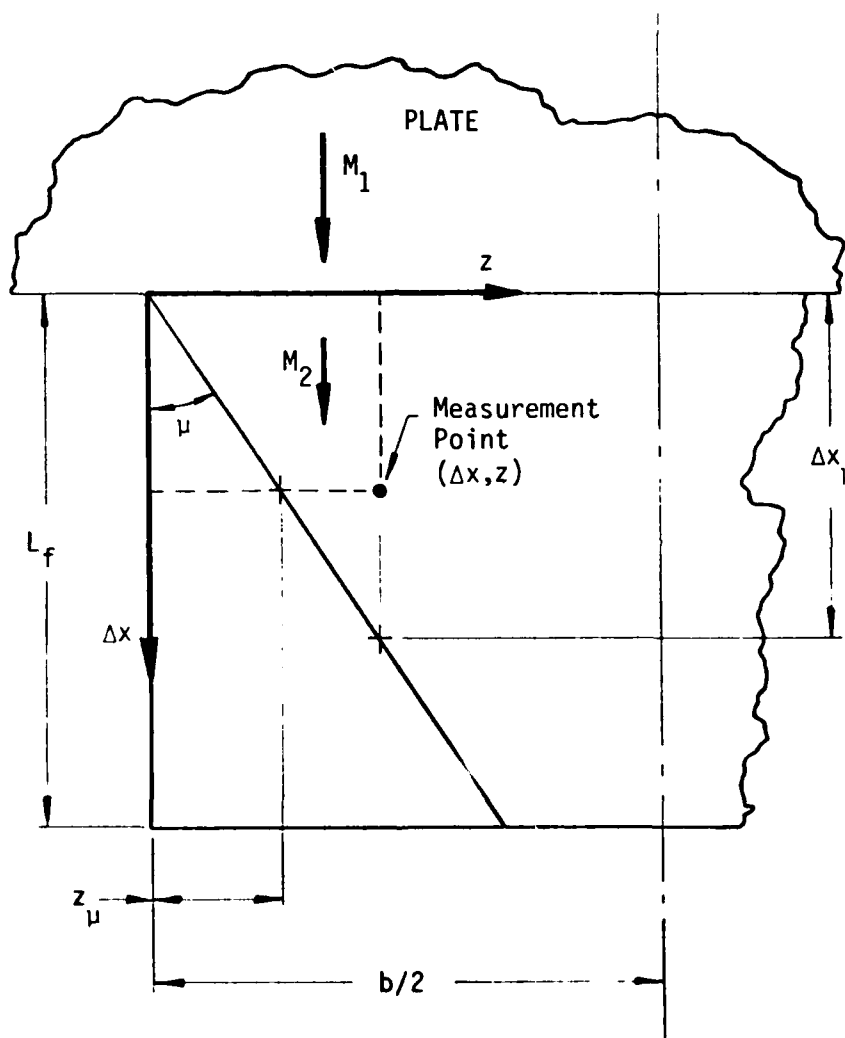

FIGURE 28. NOMENCLATURE FOR FLAP PRESSURE AND
HEAT TRANSFER DATA ANALYSIS

3.3.1 Span Effects on Centerline Distributions

The variation in the chordwise distribution of pressure along the flap centerline is shown for three different span flaps in Figures 29, 30 and 31 at deflection angles of 5, 10 and 15 degrees, respectively. (Data for the 4 in. span flap at the 15 degree deflection appeared anomolous and were omitted). For a given deflection angle, the centerline presure distributions for the three flap spans were generally quite consistent and show virtually no sensitivity to span effects (although the smallest flap, at the highest deflection angle, does show a slight span influence). In each case, however, the centerline pressures are clearly defined by the nature of the approaching boundary layer, and smoothly rise to the inviscid two-dimensional limit.

In distinct contrast to the pressure results, the influence of span variation on the chordwise distribution of heat transfer is quite significant, as illustrated in Figures 32, 33 and 34. The forward movement of the peak in the chordwise distribution appears to be related to the proximity of edge effects, and is the likely result of increases in spanwise pressure gradient which accompanied increases in deflection angle and reductions in span. A correlation of this edge effect influence is illustrated in Figure 35, where the ratio of measured Stanton number, St_1, to that recorded on the widest span flap (b_f = 5.0 in.), denoted by $(St_1)_{2D}$, is shown as a function of the chordwise approach to the Mach line emanating from the leading edge corner of the flap. Within the accuracy of the data, the effect of finite flap span appears to consistently effect a small increase in the level of the heat transfer rate over much of the centerline length.

3.3.2 Span Effects on Spanwise Distributions

The spanwise distribution of measured pressure coefficients on the flap is shown at three chord locations, for three spans and three deflection angles, in Figures 36-38. The pressure levels for the smallest span are consistently higher than those for the larger span flaps, suggesting a
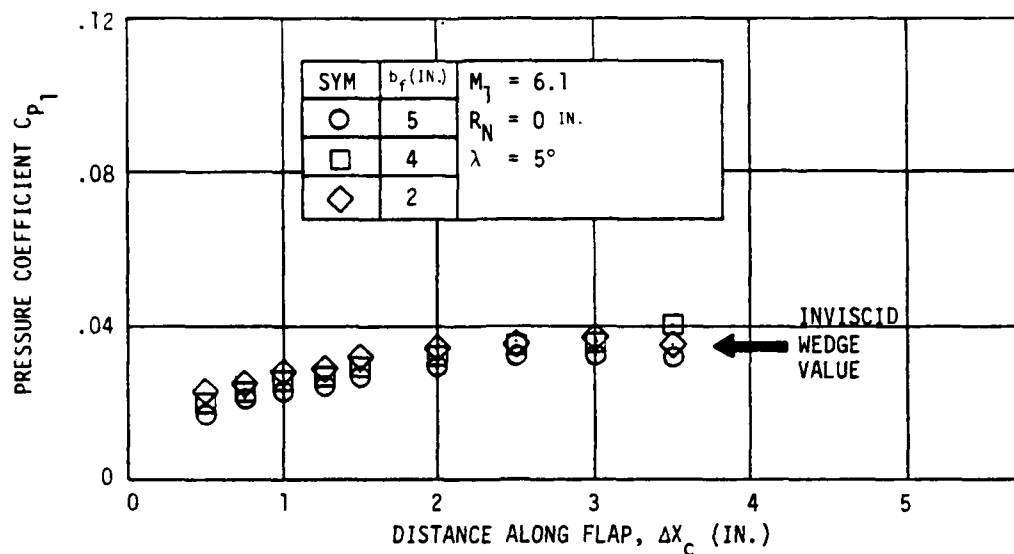
FIGURE 29.   EFFECT OF FLAP SPAN ON CENTERLINE PRESSURE
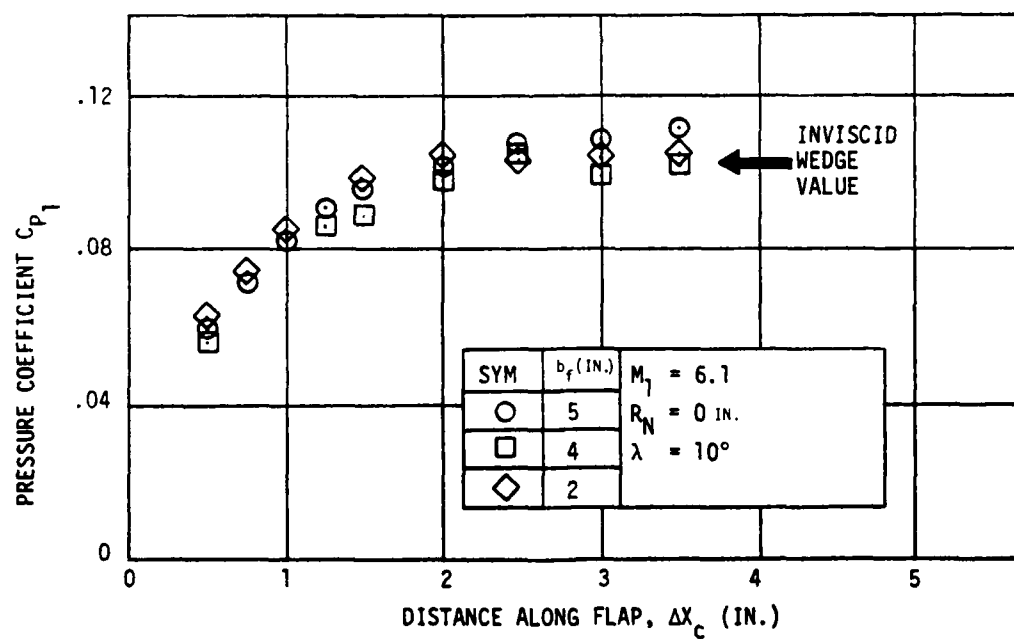DISTRIBUTION (5° DEFLECTION)

FIGURE 30.   EFFECT OF FLAP SPAN ON CENTERLINE PRESSURE
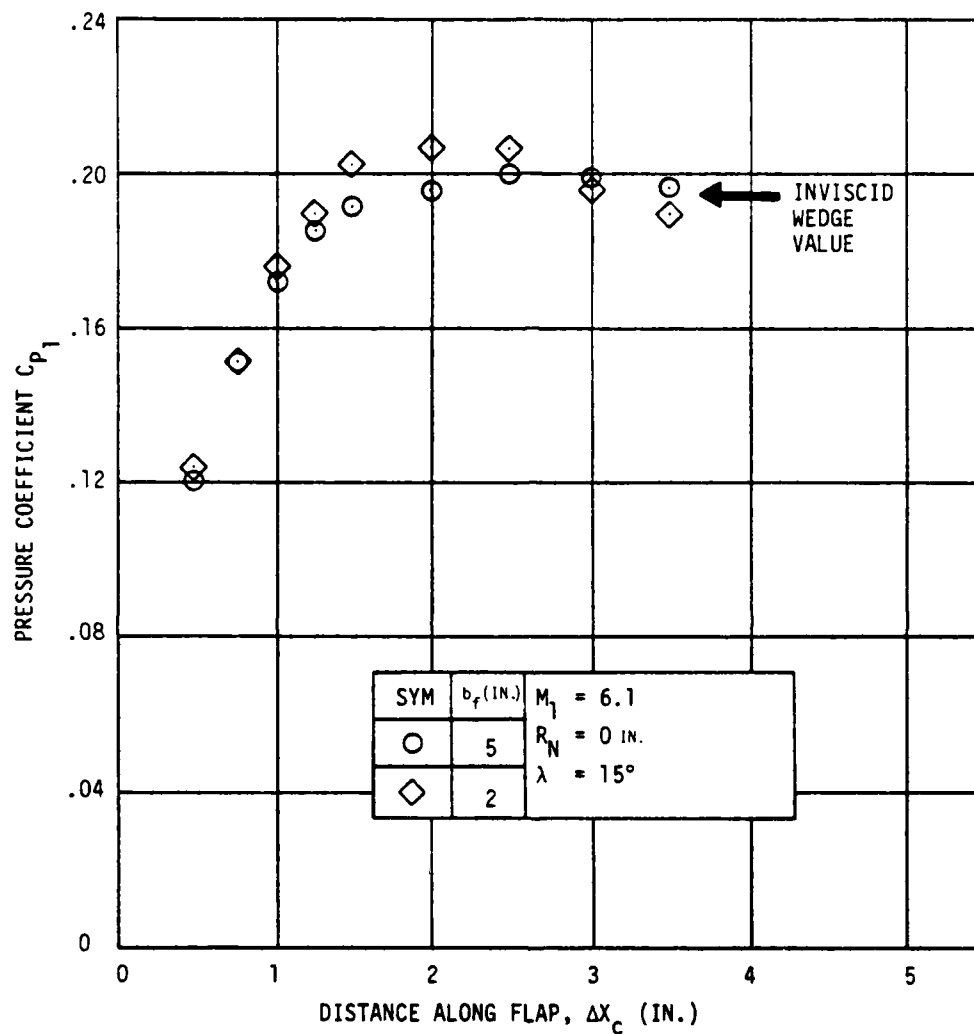DISTRIBUTION (10° DEFLECTION)

42

FIGURE 31. EFFECT OF FLAP SPAN ON CENTERLINE PRESSURE DISTRIBUTION (15° DEFLECTION)
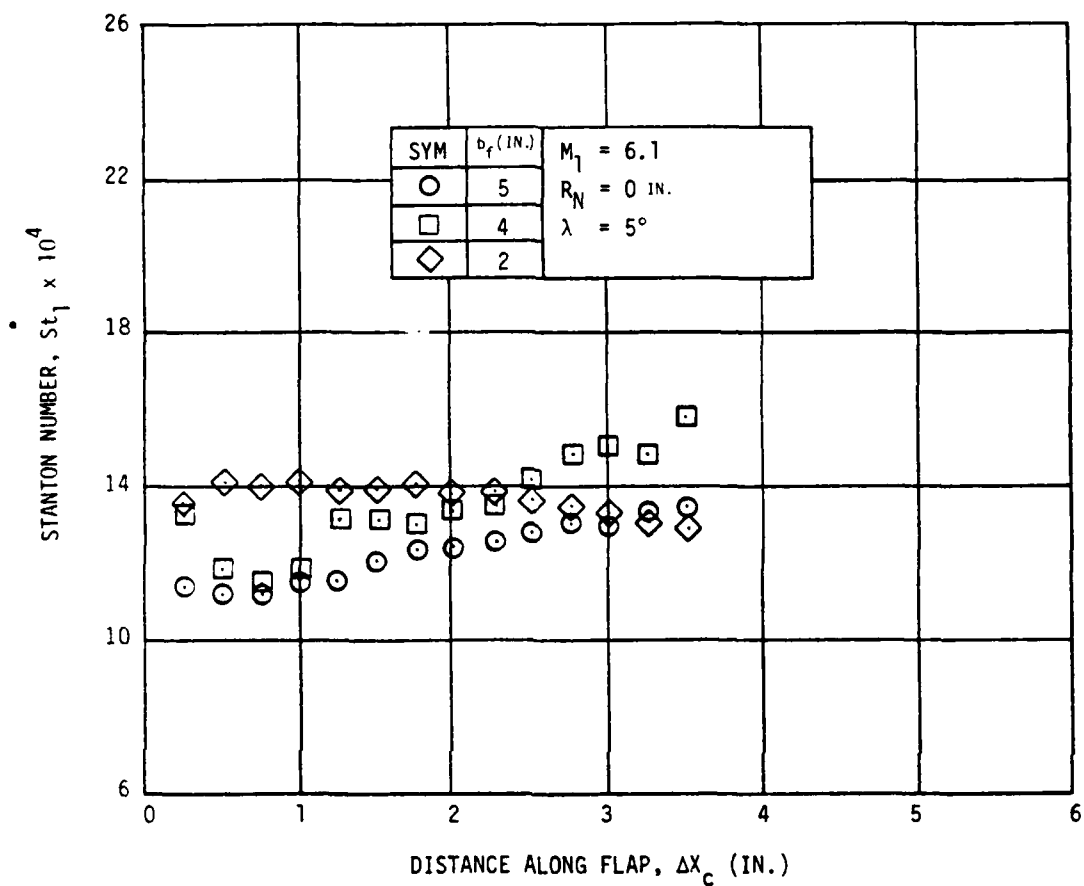
FIGURE 32.   EFFECT OF FLAP SPAN ON CENTERLINE HEATING
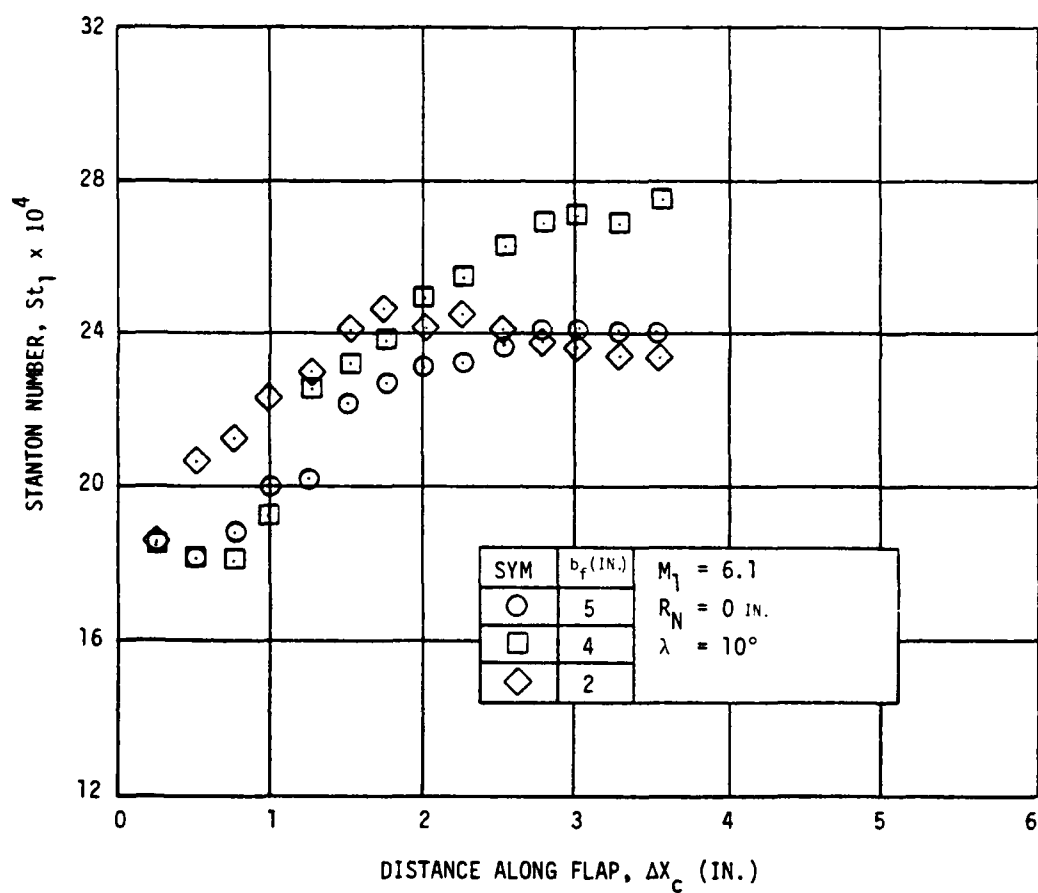DISTRIBUTION (5° DISTRIBUTION)

44

FIGURE 33. EFFECT OF FLAP SPAN ON CENTERLINE HEATING
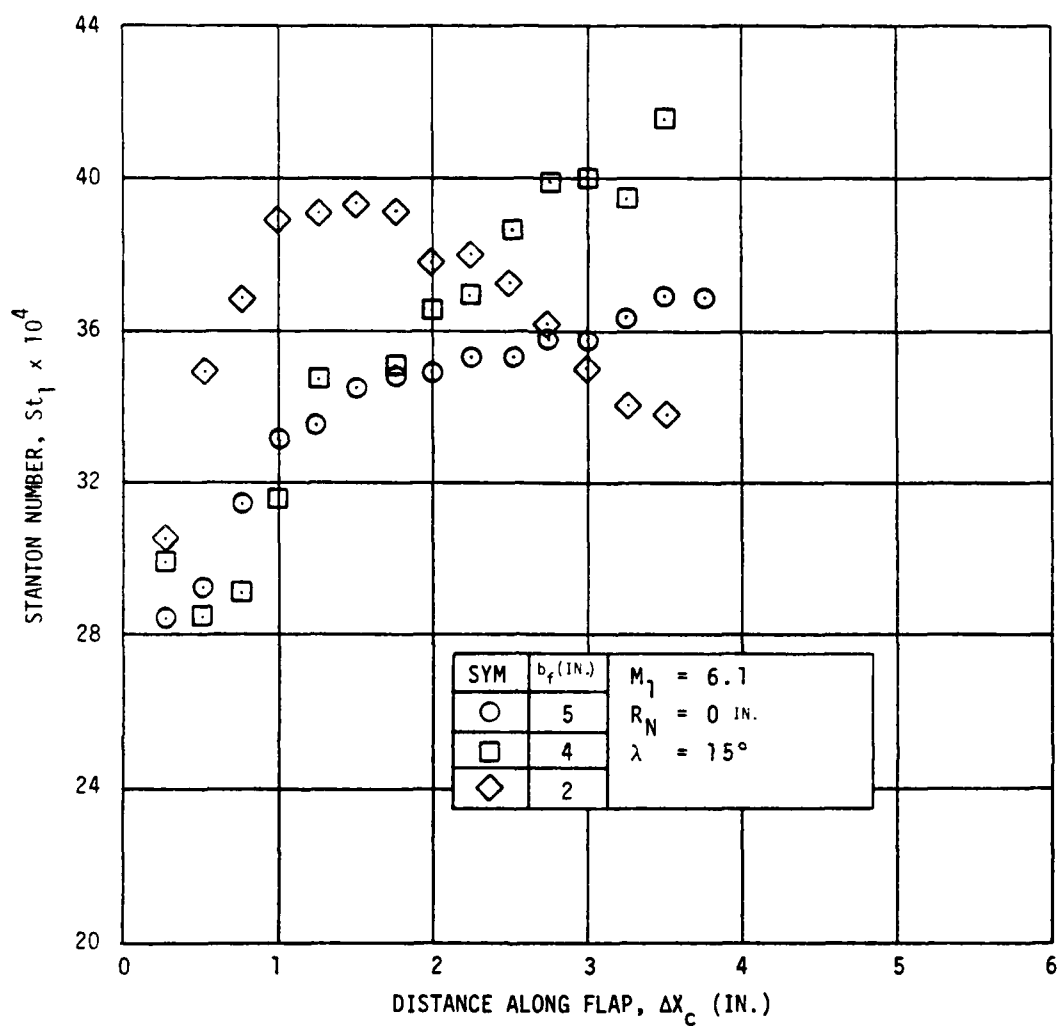DISTRIBUTION (10° DEFLECTION)

FIGURE 34.   EFFECT OF FLAP SPAN ON CENTERLINE HEATING
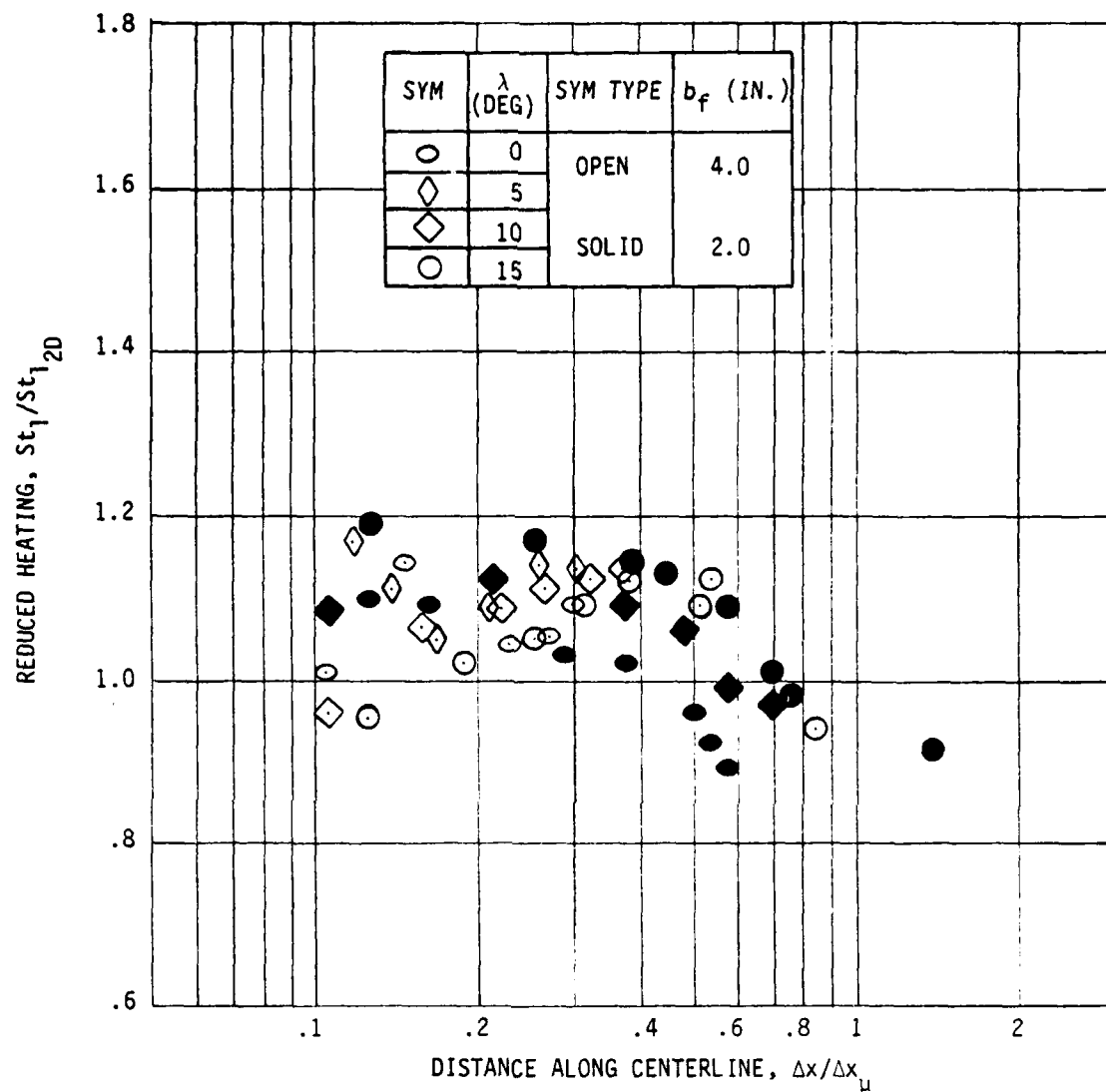DISTRIBUTION (15° DEFLECTION)

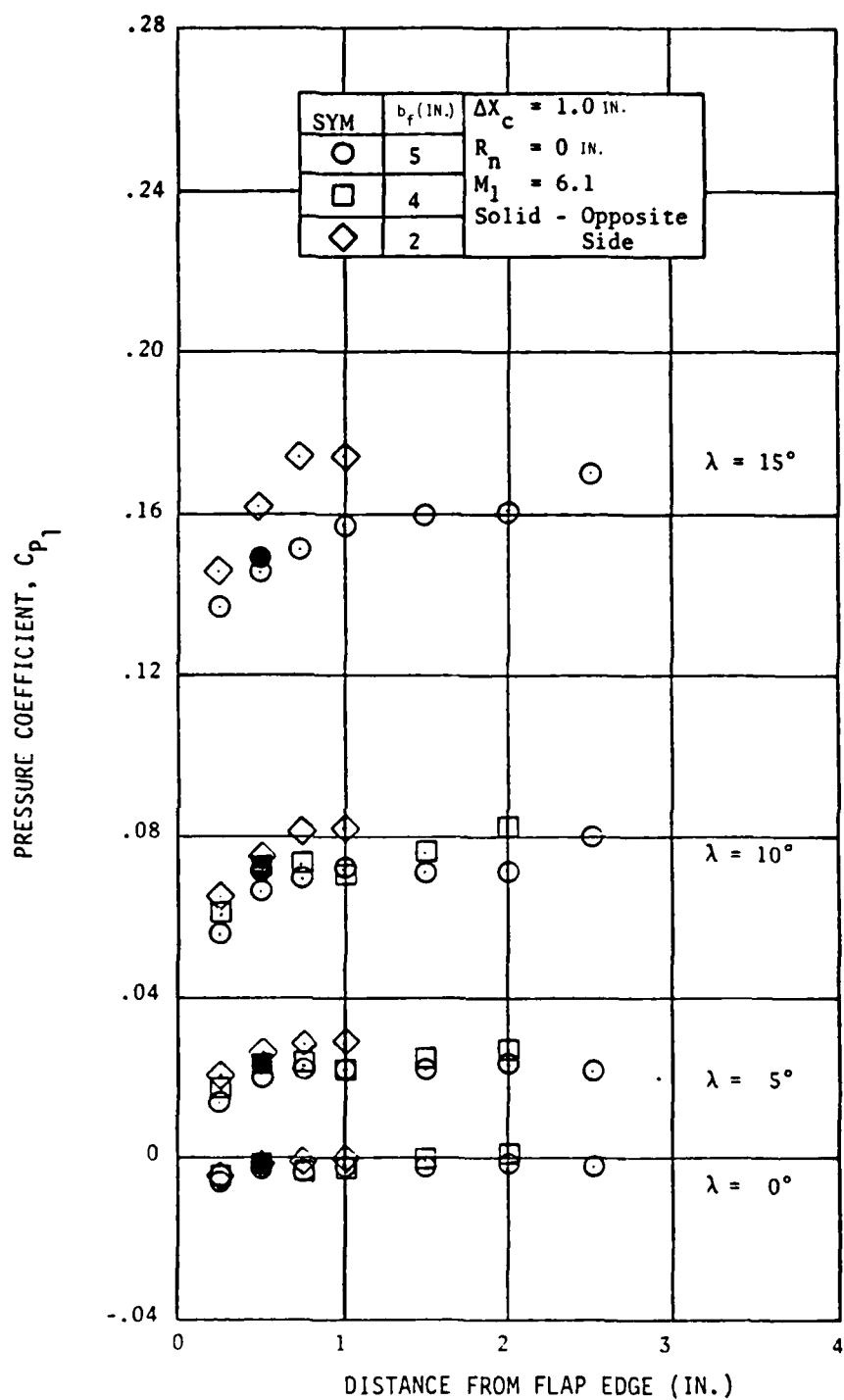FIGURE 35.   SPAN EDGE EFFECT ON FLAP CENTERLINE HEAT TRANSFER

FIGURE 36. EFFECT OF FLAP DEFLECTION ON SPANWISE PRESSURE
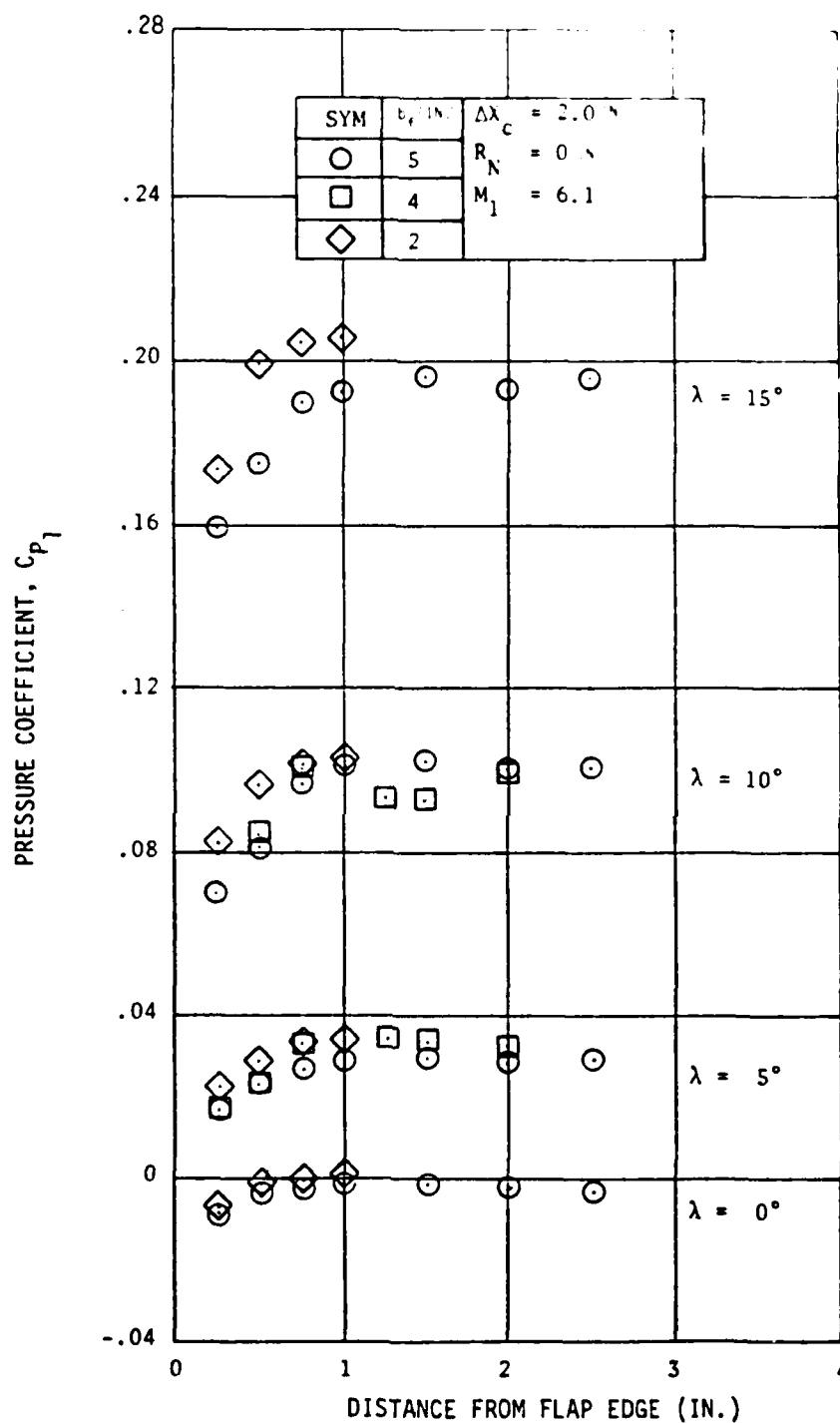DISTRIBUTIONS AT 25% CHORD STATION

FIGURE 37.   EFFECT OF FLAP DEFLECTION ON SPANWISE PRESSURE
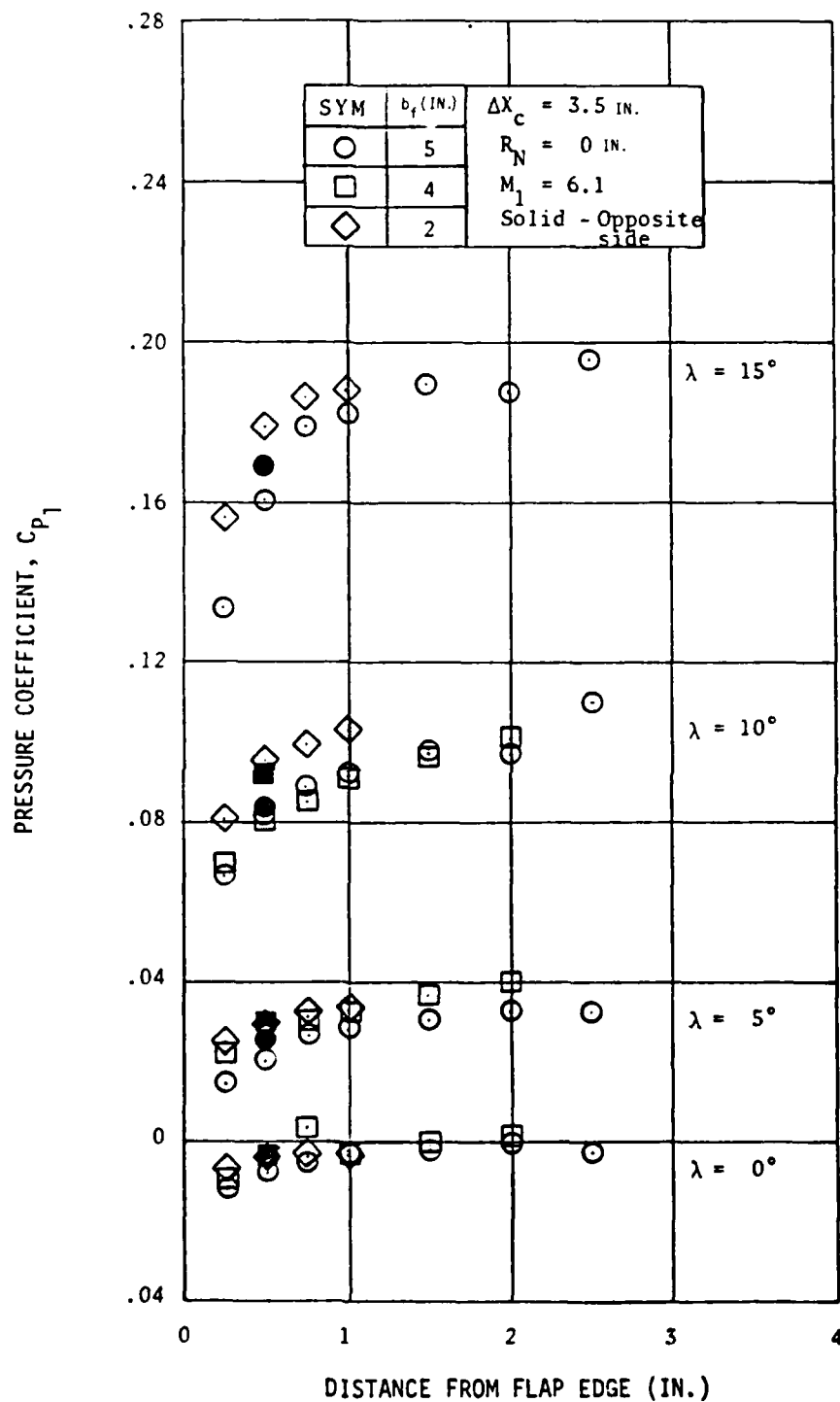DISTRIBUTIONS AT 50% CHORD STATION

49

FIGURE 38. EFFECT OF FLAP DEFLECTION ON SPANWISE PRESSURE
DISTRIBUTIONS AT 87.5% CHORD STATION

50

tendency for the shock to become more three-dimensional in nature for the small span widths. A correlation of the influence of finite span edge effects on measured spanwise pressure distributions is shown in Figure 39, where the variation in spanwise pressure coefficient (normalized by the centerline coefficient, $(C_p)_C$, at the same chord location) is shown as a function of the distance, Z, from the edge of the flap (normalized by the distance, Z_μ, of the Mach line emanating from the most forward edge of the span from the same reference location). The qualitative correlation is evident, and appears sufficiently consistent to assign first order effects in spanwise pressure variations to span edge effects. The failure of the data to reach the centerline pressure at a value of $Z/Z_\mu = 1$ suggests that the edge effects are controlled by lower valued Mach numbers within the flap boundary layer rather than the "edge" Mach number behind the flap shock. The reduction in pressure as the flap edge is approached (smaller values of Z/Z_μ) is typical of edge influences on finite span plates in two-dimensional, supersonic flow.

The spanwise distribution of heat transfer rates on the flap at three chord stations is illustrated for three spans and three deflection angles in Figures 40-42. Spanwise distributions are shown for the same chordwise stations that the pressure distributions were shown for above. A correlation of the inviscid flow edge effects on the spanwise heat transfer distribution is illustrated in Figure 43. This correlation has omitted data points from thermocouples closest to the flap edges, since nonlinearities were observed in the temperature-time output from these instruments. A comparison of these heating data with the similarly correlated pressure data of Figure 39 shows that the heating rate is less sensitive to span effects than the pressures. This behavior is consistent with expectations, in that the spanwise pressure gradient implies a thinner boundary layer (relative to the two-dimensional case) and accompanying higher heat transfer rates. In terms of overall flap thermal environments, the correlations of Figures 35 and 43 suggest that an understanding of centerline heating rate distributions provides the flap designer with adequate information to define the baseline heating environment for the entire flap.
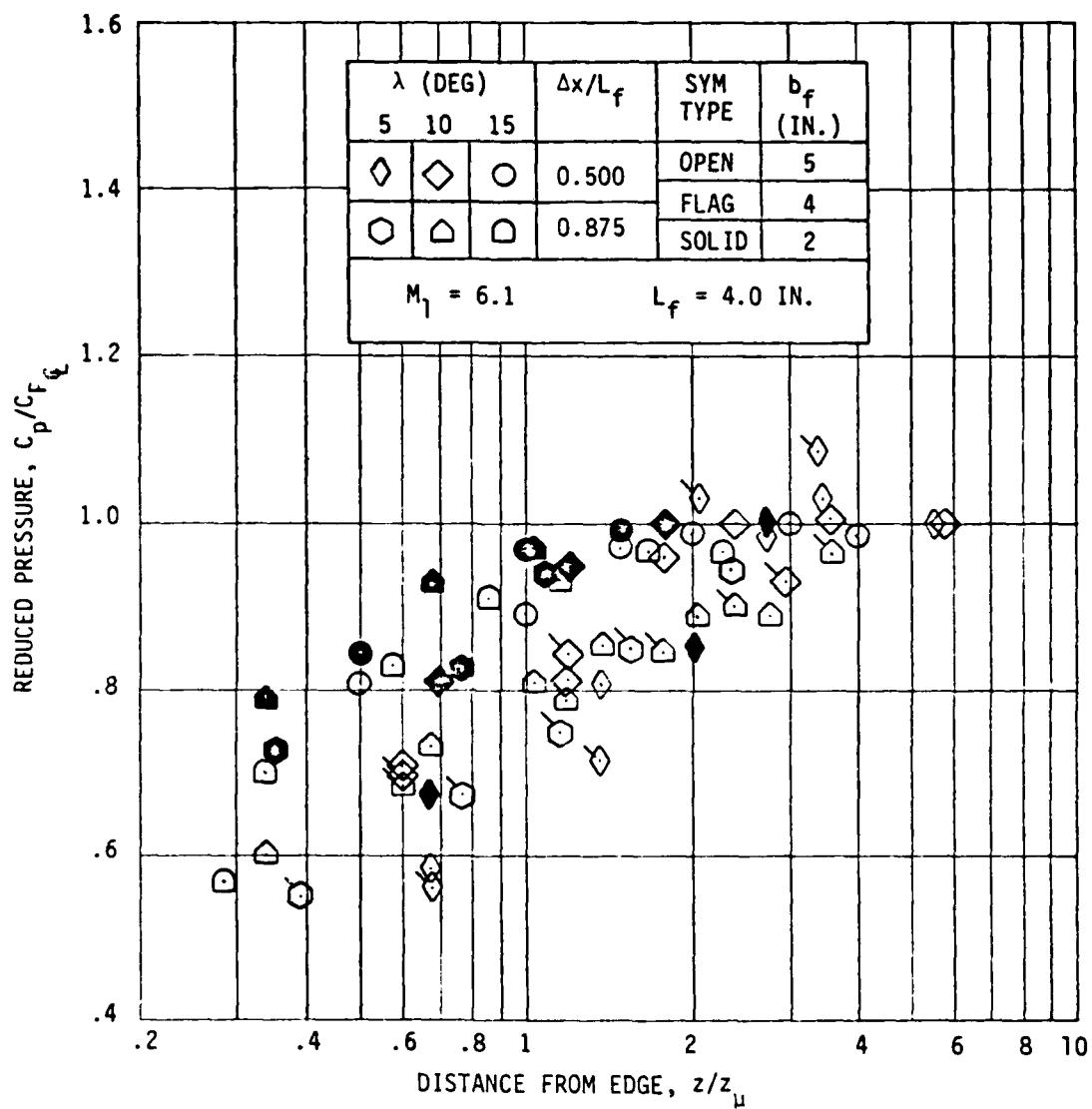
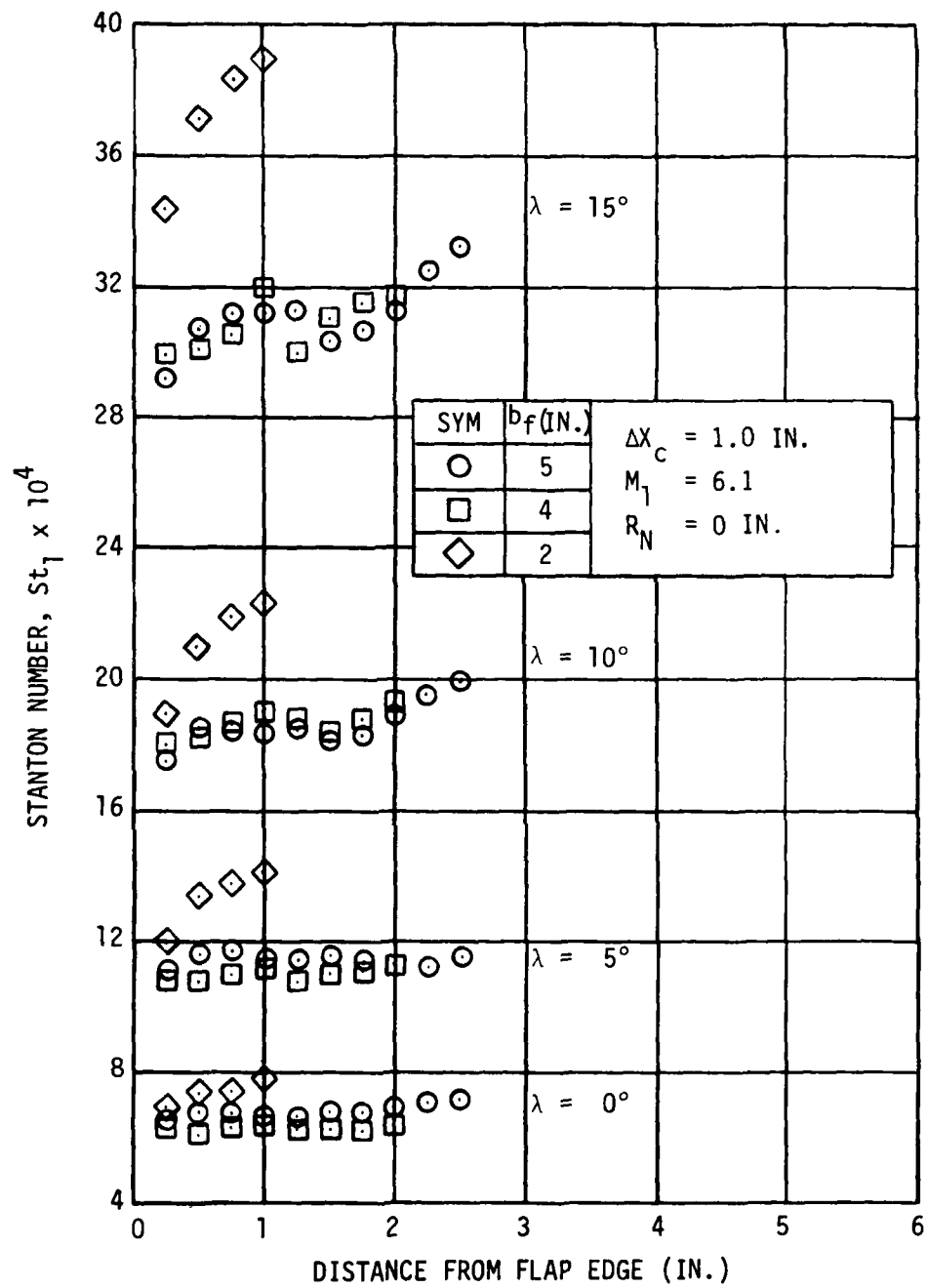FIGURE 39.   SPAN EDGE EFFECT ON SPANWISE PRESSURE DISTRIBUTION

FIGURE 40. EFFECT OF FLAP DEFLECTION ANGLE ON SPANWISE HEAT
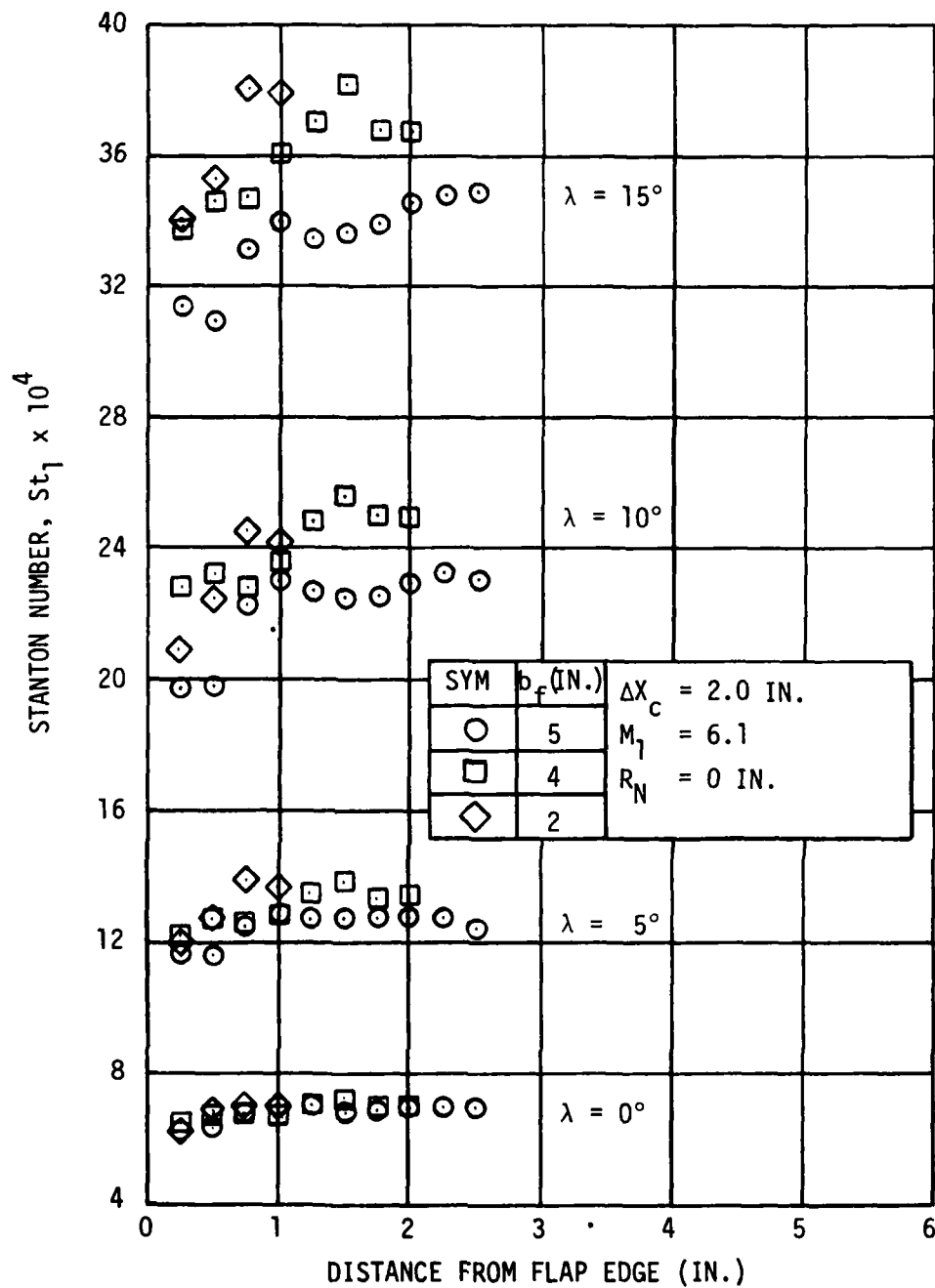TRANSFER DISTRIBUTION AT 25% CHORD STATION

FIGURE 41. EFFECT OF FLAP DEFLECTION ANGLE ON SPANWISE HEAT TRANSFER DISTRIBUTION AT 50% CHORD STATION
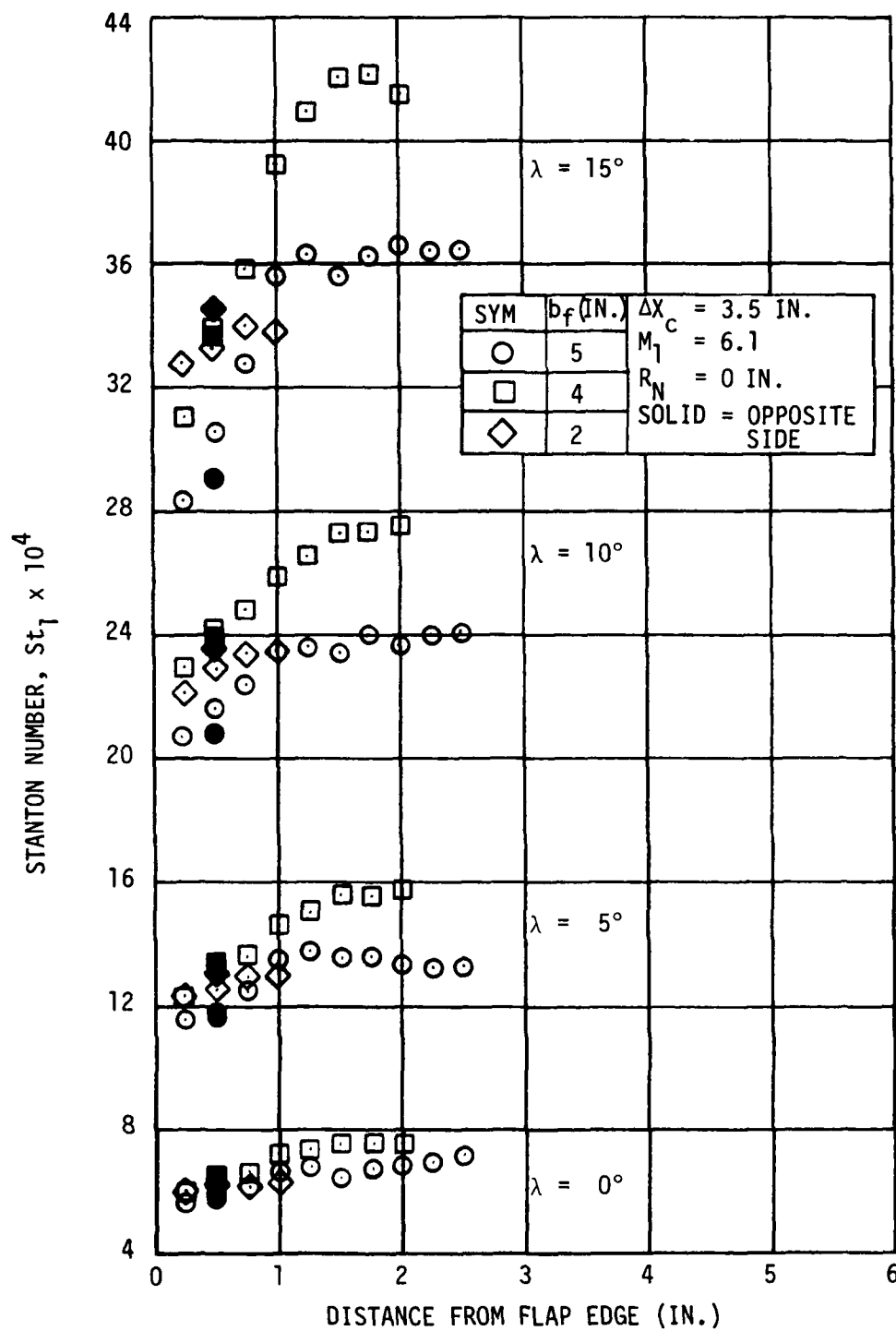
FIGURE 42. EFFECT OF FLAP DEFLECTION ANGLE ON SPANWISE HEAT
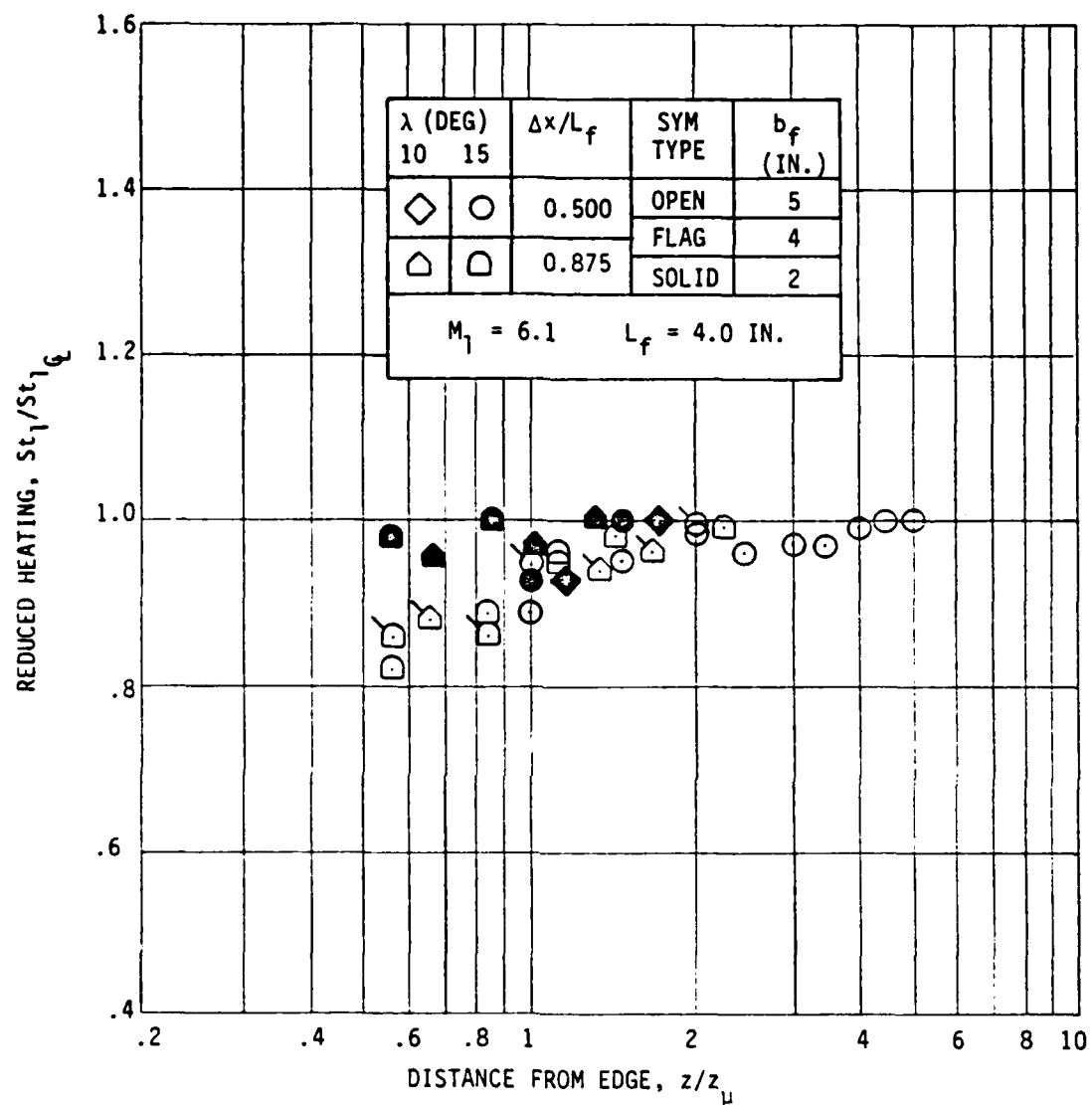TRANSFER DISTRIBUTION AT 87.5% CHORD STATION

FIGURE 43. SPAN EDGE EFFECT ON SPANWISE HEAT TRANSFER DISTRIBUTION

56

3.3.3 Span Effects on Flap Moments and Forces

Departures from ideal (inviscid, two-dimensional) flap performance caused by upstream viscous effects and by finite span effects are illustrated in Figures 44 and 45. All moments and forces are nondimensionalized by the inviscid, two-dimensional value, ($h_{2D,i}$ and $N_{2D,i}$), respectively. Measured pressure data were used to obtain flap hinge moments about the leading edge of the flap and the normal force in two ways: 1) by integrating centerline pressures only, to assess the effects of the oncoming boundary layer (dashed line); and, 2) by integration of both spanwise and chordwise distributions, to obtain the combined effects of the upstream boundary layer and the finite span. The hinge moments and forces in the later case were calculated by assuming that the measured centerline pressure existed laterally until edge influences became important and that the pressure then declined linearly to the value P_1 at the edges. Obviously, the pressure along the span edges of the flap are dependent upon the geometry of the plate on either side of the flap. In the present experiment, the plate sloped away from the primary surface at a 15 degree angle, starting at the station of the flap leading edge.

The results in Figures 44 and 45 clearly show substantial losses in flap effectiveness due to edge effects and, to a lesser extent, upstream boundary layer effects. The latter effect becomes important when the chord dimension is on the order of the approaching boundary layer thickness. In addition, the degradation in flap performance due to edge effects is a function of the flap chord, as a greater percentage of the surface is affected by the edge with increasing chord. The case where the dimensions of the chord and span are such that edge effects are important across the entire span was not addressed in the present experiments. Although the results in Figures 44 and 45 are strictly applicable only to the flow situation and flap dimensions addressed under this test program, it is apparent that flap design must properly account for the effects of both finite span and the approaching boundary layer.

3.4 Leading Edge Bluntness Effects

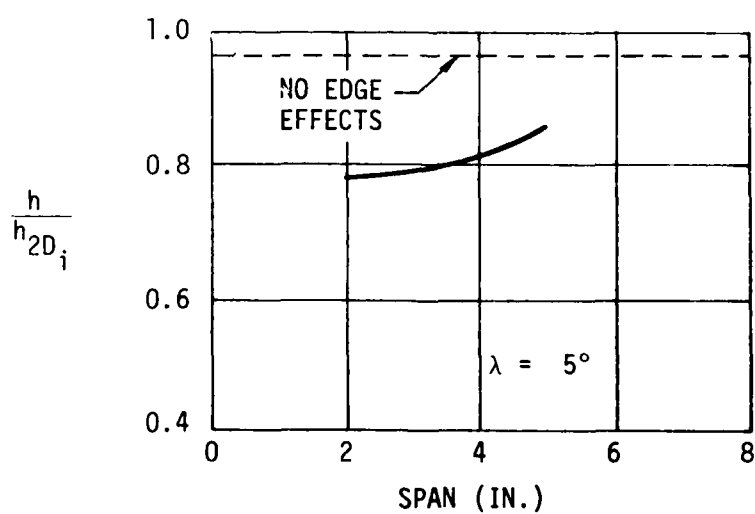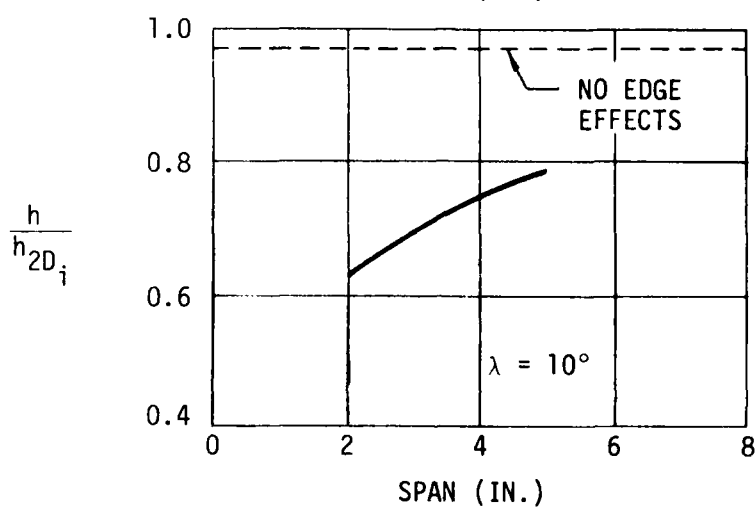Comparisons of centerline pressure and heat transfer distributions are shown in Figures 46 and 47, respectively, for leading edge bluntnesses
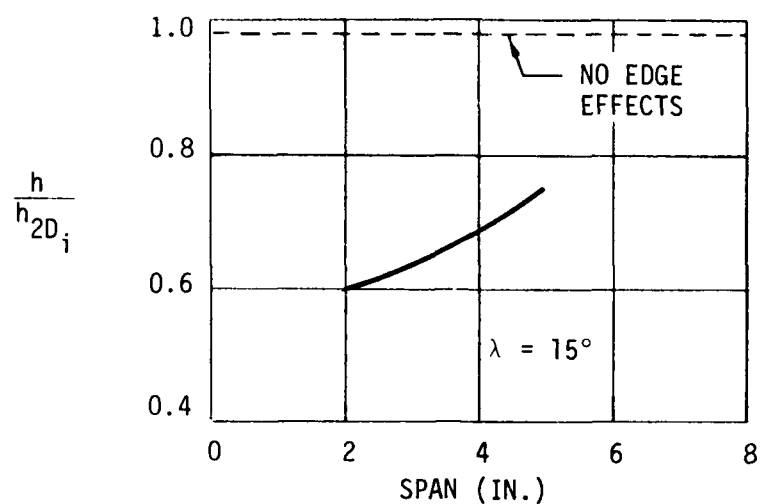
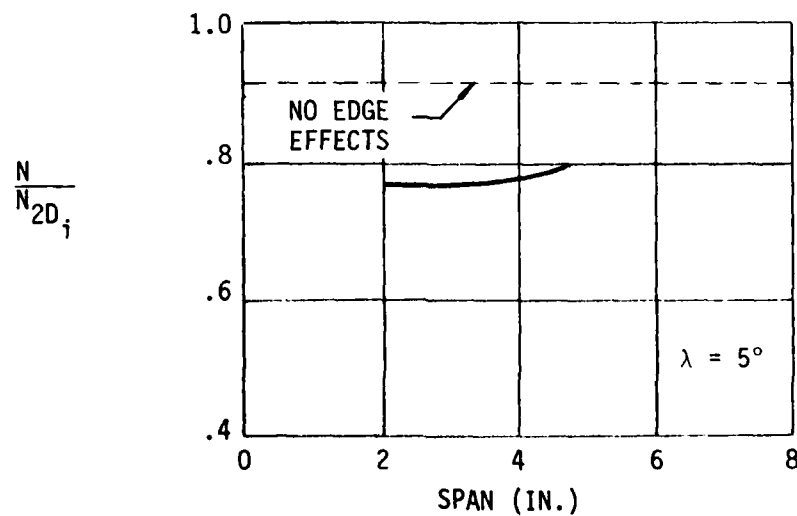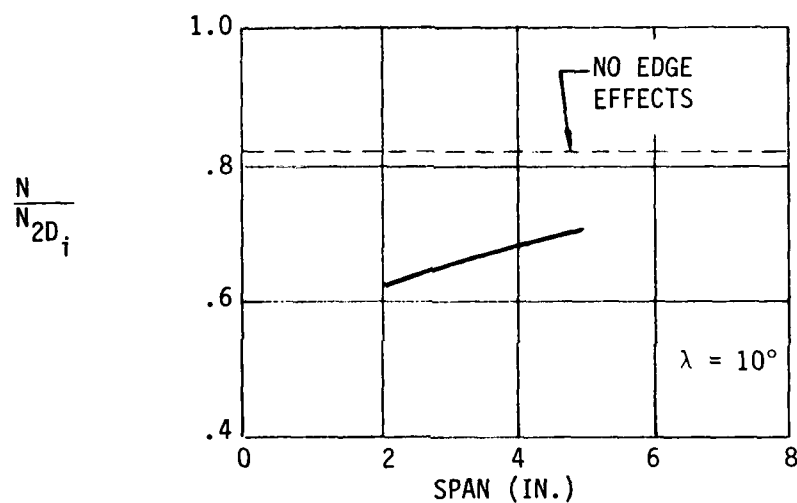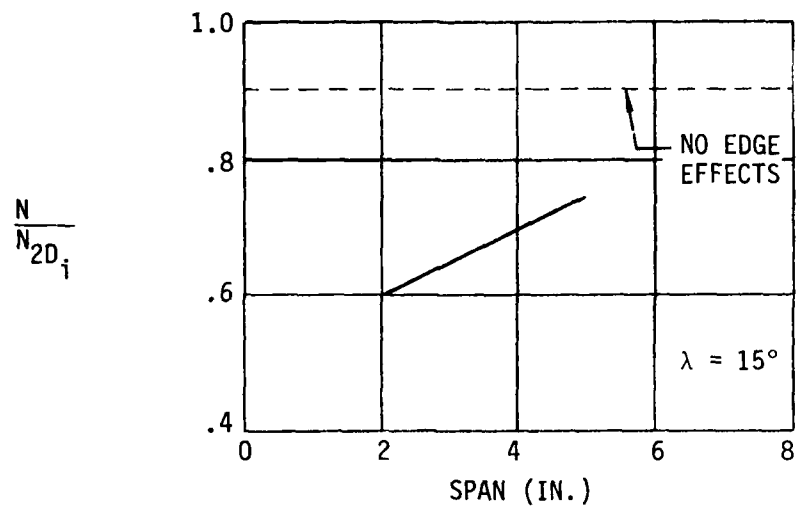FIGURE 44.   FINITE SPAN EFFECTS ON FLAP HINGE MOMENT

FIGURE 45. FINITE SPAN EFFECTS ON FLAP NORMAL FORCE
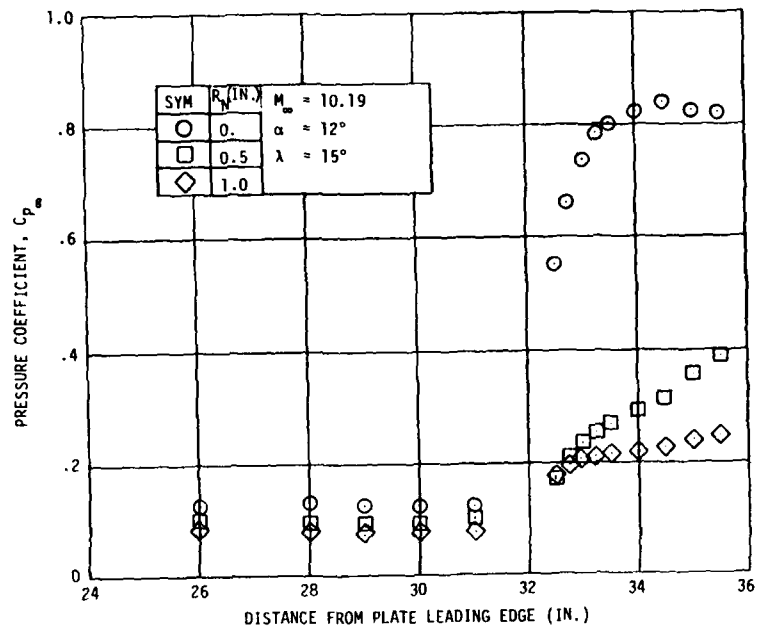
FIGURE 46.   EFFECT OF LEADING EDGE BLUNTNESS ON
CENTERLINE PRESSURE DISTRIBUTION
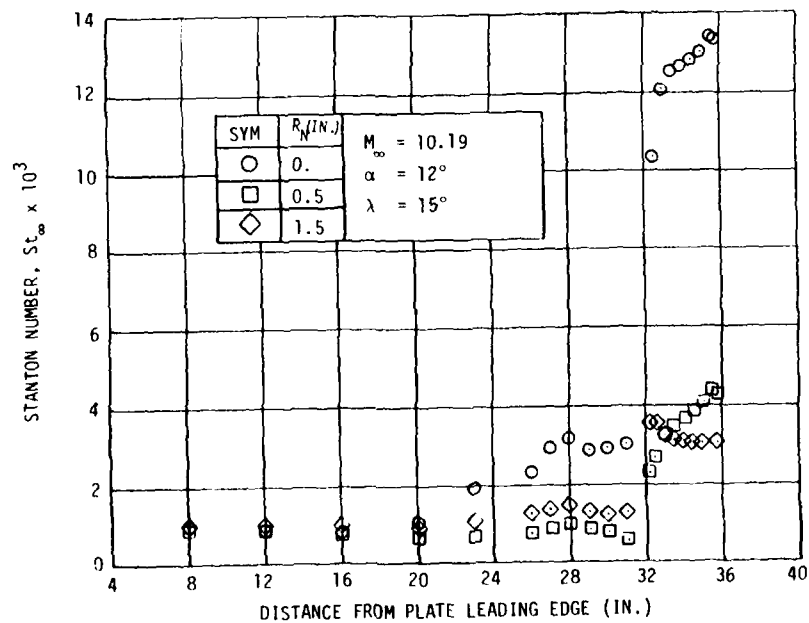
FIGURE 47.   EFFECT OF LEADING EDGE BLUNTNESS ON
CENTERLINE HEAT TRANSFER DISTRIBUTION

60

of 0, 0.5 and 1.0 in. radii. As the heat transfer data illustrate, it appears that prior to the plate/flap junction, flow was at best transitional for the 0.5 inch radius, and was probably laminar for the largest bluntness. Therefore, effects of bluntness in a turbulent boundary layer could not be assessed. However, it was found that Elfstrom's method for predicting flap surface pressures agreed very well with the data, giving greater credibility to the method for arbitrary Mach number profiles in zero pressure gradient flow. As expected, pressure recovery on the flap is much smaller for the blunted leading edges than the sharp leading edge, indicative of not only lower Mach numbers present in the boundary layer (presumably laminar for the blunted configuration) but lower edge Mach numbers because of nose bluntness.

CONCLUSIONS

Experiments were conducted at the NASA Langley Research Center Continuous Flow Hypersonic Tunnel to investigate the influence of finite span on the pressure and heat transfer distributions on flaps subjected to a hypersonic, two-dimensional flow under turbulent boundary layer conditions. The primary experiments were performed using a flap attached to a sharp leading edge flat plate which was inclined to the freestream such that the Mach number approaching the compression corner was 6.1, with a corresponding wetted length Reynolds number of 8.8×10^6. Flap angles were varied from 0 to 15 degrees and flap spans of 5, 4 and 2 inches were tested. Surface pressure and heat transfer measurements were made on the flat plate and flap, and pitot pressure surveys were obtained just upstream of the compression corner in order to characterize the approaching turbulent boundary layer.

Analysis of the data resulted in several observations and conclusions:

1. Two-dimensional, supersonic flow with a turbulent boundary layer was obtained at the compression corner of the flat plate/flap model in the NASA LaRC CFHT only when the model was inclined to the freestream flow at 12 degrees angle of attack.

2. Flap centerline pressure and heat transfer data obtained during this test series agree with previous data and with methods developed both by Elfstrom and by Coleman and Stollery, for conditions where edge effects were not present.

3. The approaching boundary layer Mach number profile is critical to the determination of the pressure and heat transfer distributions on the flap. Elfstrom's method for predicting the flap centerline pressure

distribution appears to be applicable to arbitrary upstream Mach number profiles. Although the method was derived for turbulent boundary layer flows, calculations using this approach are in general agreement with the blunted leading edge flat plate data for which the boundary layer approaching the flap was, at best, transitional. All comparisons were made for zero pressure gradient flow.

4. Edge effects can lead to substantial reductions in surface pressures (and corresponding hinge moments), but show only a small influence on heat transfer distributions.

5. Reasonable correlations of finite span effects on flap pressure and heat transfer levels can be obtained by considerations of the location of the primary expansion wave (Mach line), associated with the edge Mach number behind the flap shock, emanating from the leading edge corner of the flap.

REFERENCES

1. Dunavant, J. C., and Stone, H. W., "Effect of Roughness on Heat Transfer to Hemispherical Cylinders at Mach Numbers 10.4 and 11.4". NASA TND-3871, 1967.

2. Langley Research Staff, "Continuous Flow Hypersonic Tunnel Heat Transfer Data Reduction Procedures", Users Manual.

3. Jarrett, T. W., Cassel, L. A., and McMillen, L. D., "Finite Span Effects on Flap Heating and Effectiveness in a Turbulent Boundary Layer - Test Data Report", AFWAL-TM-80-62-FIMG, April 1980.

4. Bertram, M. H., and Neal, L. Jr., "Recent Experiments in Hypersonic Turbulent Boundary Layers", NASA TM X-56335, 1965. (Also AGARD Specialists' Meeting on Recent Developments in Boundary-Layer Research, Naples, Italy, May 10-14, 1965.)

5. van Driest, E. R., "Turbulent Boundary Layers in Compressible Fluids", JAS, vol. 18, no. 3, 1951, pp. 145-160.

6. Dunavant, J. C., Private Communication.

7. Pate, S. R., "Transition Reynolds Numbers on Sharp Slender Cones", AIAA Journal, vol. 9, no. 6, pp. 1082-1090, June 1971.

8. Pate, S. R., and Schueler, C. J., "Radiated Aerodynamic Noise Effects on Boundary Layer Transition in Supersonic and Hypersonic Wind Tunnels", AIAA J, vol. 7, no. 3, 1969, pp. 450-457.

9. Potter, J. L., and Whitfield, J. D., "Effect of Unit Reynolds Number, Nose Bluntness, and Roughness on Boundary Layer Transition", AEDC-TR-60-5, 1960; also JFM, vol. 12, 1962, pp. 501-535.

10. White, F. M., "Viscous Fluid Flow", McGraw-Hill, p. 627, 1974.

11. Hopkins, E. J., Keener, E. R., and Dwyer, H. A., "Turbulent Skin Friction and Boundary Layer Profiles Measured on Non-Adiabatic Flat Plates at Hypersonic Mach Numbers", AIAA Paper 71-167, 1971.

12. Cebeci, T., and Smith, A.M.O., "Analysis of Turbulent Boundary Layers", Academic Press, N. Y., 1974.

13. Throckmorton, D. A., "Pressure Gradient Effects on Heat Transfer to Reusable Surface Insulation Tile-Array Gaps", NASA TND-7939, August 1975.

14. Thomke, G. J., and Roshko, A., "Incipient Separation of a Turbulent Boundary Layer at High Reynolds Number in Two-Dimensional Supersonic Flow over a Compression Corner", NASA CR-73308, 1969.

15. Elfstrom, G. M., "Turbulent Hypersonic Flow at a Wedge-Compression corner", J. Fluid Mechanics, vol. 53, part 1, pp. 113-127, 1972.

16. Coleman, G. T., and Stollery, J. L., "Heat Transfer From Hypersonic Turbulent Flow At a Wedge Compression Corner", J. Fluid Mechanics, vol. 56, part 4, pp. 741-752, 1972.

17. Holden, M. S., "Shock Wave-Turbulent Boundary Layer Interaction in Hypersonic Flow", AIAA Paper 72-74, January 1972.

18. Holden, M. S., "Shock Wave-Turbulent Boundary Layer Interaction in Hypersonic Flow", AIAA Paper 77-45, January 1977.

19. Elfstrom, G. M., "Turbulent Separation In Hypersonic Flow", Imperial College, University of London Acro Report 71-16, Sept. 1971.

20. Rose, W. C., Murphy, J. D., and Watson, E. C., Interaction of an Oblique Shock Wave With a Turbulent Boundary Layer", AIAA Journal vol. 6, no. 9, p. 1796, 1968.

21. Gray, D. J., and Rhudy, R. W., "Investigation of Flat-Plate Aspect Ratio Effects on Ramp Induced, Adiabatic, Boundary Layer Separation at Supersonic and Hypersonic Speeds", Arnold Engineering Development Center Report AEDC-TR-70-235, March 1971.